HHS Public Access

Author manuscript

Cell Rep. Author manuscript; available in PMC 2024 February 05.

Published in final edited form as:

Cell Rep. 2023 November 28; 42(11): 113370. doi:10.1016/j.celrep.2023.113370.

Disruptions in cell fate decisions and transformed enteroendocrine cells drive intestinal tumorigenesis in *Drosophila*

Maria Quintero[1], **Erdem Bangi**[1,2,*]

[1]Department of Biological Science, Florida State University, Tallahassee, FL 32304, USA

[2]Lead contact

SUMMARY

Most epithelial tissues are maintained by stem cells that produce the different cell lineages required for proper tissue function. Constant communication between different cell types ensures precise regulation of stem cell behavior and cell fate decisions. These cell-cell interactions are often disrupted during tumorigenesis, but mechanisms by which they are co-opted to support tumor growth in different genetic contexts are poorly understood. Here, we introduce PromoterSwitch, a genetic platform we established to generate large, transformed clones derived from individual adult *Drosophila* intestinal stem/progenitor cells. We show that cancer-driving genetic alterations representing common colon tumor genome landscapes disrupt cell fate decisions within transformed tissue and result in the emergence of abnormal cell fates. We also show that transformed enteroendocrine cells, a differentiated, hormone-secreting cell lineage, support tumor growth by regulating intestinal stem cell proliferation through multiple genotype-dependent mechanisms, which represent potential vulnerabilities that could be exploited for therapy.

Graphical Abstract

*Correspondence: ebangi@bio.fsu.edu.

AUTHOR CONTRIBUTIONS

Conceptualization, supervision, funding acquisition, E.B.; investigation, visualization, M.Q.; methodology, formal analysis, writing, E.B. and M.Q.

DECLARATION OF INTERESTS

The authors declare no competing interests.

SUPPLEMENTAL INFORMATION

Supplemental information can be found online at https://doi.org/10.1016/j.celrep.2023.113370.

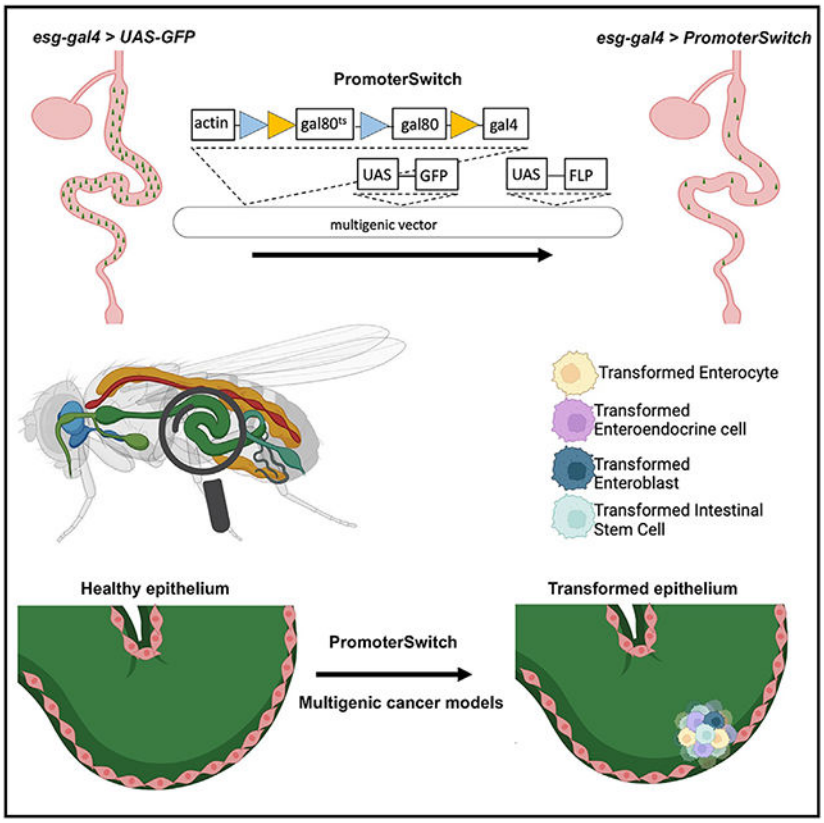

In brief

Quintero and Bangi use a genetic tool to show that cancer-driving genetic alterations disrupt cell fate decisions in the adult fly intestine, resulting in tumor-like growths that capture the cell-type heterogeneity of cancer. They also identify a tumor-promoting role for hormone-secreting enteroendocrine cells mediated by multiple genotype-dependent mechanisms.

INTRODUCTION

Precise regulation of stem cell behavior and cell fate decisions is critical to maintaining tissue integrity and homeostasis. Stem cell proliferation, self-renewal, and differentiation are coordinated by a host of intrinsic, lineage-specific factors and extrinsic signals mediating communication among cells that make up a tissue and its microenvironment.[1] Their disruption can alter the relative abundance of different cell lineages within a tissue and interfere with its ability to appropriately respond to injury, infection, environmental stresses, and the emergence of cells with cancer-driving genomic alterations, resulting in tissue dysfunction, overproliferation, and cancer.

Most solid tumors, including colon tumors, are composed of all cell types typically found in their tissue of origin, although transformed cells often have different intrinsic properties compared with their wild-type counterparts.[2-4] Multilineage differentiation within tumors is a crucial contributor to intratumor cellular heterogeneity and can also have an impact on drug response, as sensitivities of different cell lineages to chemotherapy vary.[5] During

tumorigenesis, the homeostatic cell-cell communication mechanisms that ensure tissue integrity and function are not only disrupted but can also be co-opted to support tumor growth. Molecular mechanisms underlying interactions among transformed cell lineages and their wild-type neighbors and their contributions to tumorigenesis are poorly understood. Furthermore, most tumors carry concurrent alterations in multiple genes, and there is extensive genetic heterogeneity among tumors of the same type.[6-8] As a result, the specific genomic landscape of a tumor cell will determine not only its intrinsic properties and behavior but also the extracellular signals it produces to communicate with its neighbors and how it responds to its environment.

The intestinal epithelium is one of the most rapidly renewing tissues in the body and serves as a relevant paradigm for studying stem cell regulation and epithelial homeostasis.[9,10] Both the *Drosophila* intestine and the mammalian intestine are highly regenerative organs, with intestinal stem cells (ISCs) that produce two broad categories of differentiated cell types with conserved functions and transcriptional profiles[11-14]: absorptive enterocytes (ECs) and hormone-producing enteroendocrine cells (EEs). Many aspects of interactions between the intestinal epithelium and its microenvironment, including the muscle, mesenchymal cells, immune/blood cells, and oxygen-transporting tracheal system, have also been captured in *Drosophila*.[11-13,15-19]

Intestinal cells use several highly conserved signaling pathways to communicate with one another,[17,20] primarily through secreted ligands from differentiated EEs and ECs to regulate ISC behavior.[21-26] EEs have also been detected in a significant fraction of colorectal carcinomas.[27] Notably, a particular EE subtype restricted to intestinal crypts[28] close to ISCs and expressing the peptide hormone TAC1 is associated with worse prognosis in colorectal cancer patients and lower survival rates following surgery.[29,30] EEs are thought to promote tumorigenesis by creating an environment conducive to excessive proliferation through the hormones they secrete.[31,32] However, the mechanisms underlying this tumor-promoting effect remain unknown, given the numerous peptide hormones expressed by EEs and their pleiotropic effects.

Like their human counterparts, EEs in the *Drosophila* intestine secrete many peptide hormones essential in intestinal physiology and homeostasis.[33] The contribution of the EE hormone Tachykinin (Tk; the *Drosophila* TAC1) to stem cell regulation has been well established in *Drosophila*,[24-26] but a role during intestinal tumorigenesis has not been demonstrated. ISC tumors in *Drosophila* depend on secreted signals from wild-type ECs and non-autonomous JNK and Hippo signaling.[34-38] As human tumors typically have high numbers of transformed differentiated cells, which may also secrete these niche signals, whether they are as dependent on non-autonomous signals from the surrounding epithelium remains to be determined.

We have previously used colon tumor sequence data available from The Cancer Genome Atlas (TCGA) to generate a panel of multigenic *Drosophila* models that capture the genomic landscape of colorectal cancer[39,40] and leveraged fundamental similarities between the mammalian and the *Drosophila* intestine[20,41,42] to study intestinal transformation by genetically manipulating *Drosophila* orthologs of genes recurrently mutated in human colon

tumors.[43,44] These models focused on five genes, APC, KRAS, TP53, SMAD4, and PTEN, which lead to the deregulation of the Wnt, RAS/MAPK, DNA-damage-response/apoptosis, TGF-β, and PI3K pathways, respectively.[45,46] APC, TP53, and KRAS are the three most frequently mutated genes in human colon tumors,[39] making the KRAS TP53 APC mutation profile a common colorectal cancer landscape and a useful base model. Our collection also includes two models that introduce additional genetic complexity to the KRAS TP53 APC background by modeling loss of TGF-β signaling (KRAS TP53 SMAD4 APC) or activation of the PI3K pathway (KRAS TP53 PTEN APC), which represent two other recurrent events in colon cancer. In previous studies, these models captured critical aspects of tumorigenesis and showed that many tumor phenotypes are emergent features of interactions between multiple transgenes.[43,44]

Exploring cell-cell interactions and fate decisions during intestinal transformation requires studying discrete clones originating from individual cells of defined lineages and capturing the cell-lineage heterogeneity found in colon tumors. Targeting individual cell lineages using cell-type-specific promoters can result in the transformation of a large number of cells in the intestine; cell-type-specific promoters mediating transgene expression can become silenced as transformed cells attempt to differentiate. For instance, *esg-gal4*, a gal4 line targeting adult stem and progenitor cells,[47,48] is commonly used to study intestinal homeostasis and tumorigenesis in *Drosophila*.[49] However, as targeted cells differentiate and lose *esg-gal4* expression, gal4-driven genetic manipulations become silenced. To get around this problem, lineage-tracing tools like the *esg^{ts} F/O* system that targets all stem/progenitor cells and all their progeny have been established.[23,49] Given the rapid rate of midgut epithelial turnover, where the entire epithelium can be replaced in as little as 4 days,[23,49,50] targeting multigenic cancer models to all ISCs and their subsequent progeny rapidly transforms the entire epithelium, compromising tissue integrity and resulting in organismal lethality. Genetic tools like MARCM (Mosaic Analysis with a Repressible Marker) that combine the UAS-Gal4 system with a heat-shock-inducible FLP recombinase (*hs-FLP*) can be used to target a subset of cells expressing a gal4 of interest.[51] Still, UAS-driven genetic manipulations remain dependent on the expression of the initial cell-type-specific gal4 line and can be lost as a result of differentiation or cell fate changes. Therefore, a modified lineage-tracing tool that targets only a small subset of any cell lineage of interest is necessary to generate and study discrete clones and study cell-cell interactions at the clone boundary.

To overcome these challenges, we established a new genetic platform, PromoterSwitch (PS), to generate a small number of clones derived from individual stem/progenitor cells. These clones recapitulate multiple key indicators of oncogenic transformation and cell-lineage heterogeneity observed in human colon tumors. We find genotype-dependent differences in the relative abundance of the differentiated, hormone-secreting EE lineage and disruptions in stem cell regulation and EE fate determination. Last, we identify a tumor-promoting role for the transformed EEs with distinct, genotype-dependent mechanisms. These findings provide insights into cell fate decisions and cell-cell communication during tumor progression in a whole-tissue context and offer a possible mechanism for the clinical observation that colon tumors with high numbers of EEs are more aggressive with a worse prognosis.[29,30]

RESULTS

Generating transformed clones in the adult *Drosophila* intestine using PromoterSwitch

Here, we introduce PS (Figures 1A and 1B), an intersectional design inspired by the CoinFLP method[52] that combines the Gal4/UAS/Gal80(ts) system, a repressible targeted expression system for tissue-specific genetic manipulations in *Drosophila*,[53,54] and the site-directed FLP/FRT recombination method that uses the FLP recombinase to excise any DNA sequence flanked by its FLP recognition target (FRT) sites.[55] It allows the targeting of transgene expression to a small subset of cells expressing a cell-type-specific gal4. Once FLP recombinase expression is induced using a cell-type-specific gal4, most initially targeted cells undergo a site-specific recombination event that results in ubiquitous Gal80 expression, which permanently shuts down the UAS-Gal4 system (Figure 1A). At the same time, a small subset permanently locks in transgene expression by switching to the ubiquitous *actin* promoter to drive gal4 expression through a different site-specific recombination event. As this "promoter switch" occurs only in initially targeted cells, cell-type specificity of genetic manipulations is preserved. To simplify the genetic background of our experimental animals and allow the introduction of additional transgenes for mechanistic studies, we consolidated the transgenes required for the PS design into a single plasmid using our multigenic vector platform[56] (Figures 1B, S1A, and S1B).

This flexible platform can be combined with any gal4 of interest to achieve more refined and permanent genetic manipulations. For instance, when crossed to *esg-gal4*, expressed in intestinal stem and progenitor cells,[47,48] PS results in permanent targeting of approximately 10% of the *esg-gal4*-positive cells (Figures 1C and 1D). Over time, many of the cells that have undergone the switch to the *actin* promoter form small clones, indicating that gal4 expression has been permanently activated in these cells and their progeny, regardless of their differentiation status (Figure 1E). Without PS, GFP expression is present only in the stem and progenitor cells at all time points (Figures 1D and 1E).

We used the PS design and *esg-gal4* to target our multigenic combinations (Figures 1F and 1G) to a small number of individual cells in the adult intestine. We focused our analysis on three models that represent commonly observed colon tumor genome landscapes. Our RPA model combines oncogenic KRAS with loss of TP53 and APC, the three most frequently mutated genes in colon tumors, representing a commonly observed mutation profile. The RPPA and RPMA models incorporate PTEN and SMAD4 loss to model PI3K pathway activation and loss of TGF-β signaling, respectively, which are frequently observed in colon tumors as well, adding two more complex mutation profiles to our study.

Targeting RPA, RPPA, and RPMA to the stem and progenitor cells of the adult intestine using PS and *esg-gal4* resulted in multicellular clones that were significantly larger than GFP-only control clones (Figures 1H-1L). By substantially reducing the number of clones per intestine, the PS platform allowed us to follow clone growth and transformation for 2 weeks, after which experimental clones started to compromise tissue integrity and function, resulting in organismal lethality.

During a 2-week period of induction, we noted significant differences in the growth rates of clones with different genotypes (Figure 1H): RPPA clones showed the fastest growth, with RPA clones taking twice as long to reach a comparable size. While still larger than control clones, RPMA clones did not grow as large as RPA or RPPA. These differences might reflect the more nuanced and paradoxical role of TGF-β signaling in cancer, where it can be tumor suppressive and tumor promoting in the same tumor type at different stages of tumorigenesis.[57]

We also found that a significantly higher fraction of cells targeted with RPA, RPPA, and RPMA gave rise to multicellular clones compared with GFP-only controls (Figure S1C), suggesting that these cancer-driving multigenic combinations increase the proliferation rate or potential of targeted cells. The numbers of GFP-positive cells and clones at earlier time points were similar across all experimental and control genotypes, indicating the frequencies of the desired promoter switch event were comparable across all genotypes (Figure S1D).

Consistent with their larger size, RPA, RPPA, and RPMA clones had higher proliferation rates than GFP-only control clones as evaluated by the mitotic marker phosphate-Histone 3 (pH3) (Figures 2A-2F). We also observed an increase in mitotic cells in the surrounding wild-type epithelium (Figure 2G). Even though this increase was statistically significant only in intestines with RPA clones (Figure 1G), these findings suggest a non-autonomous proliferative response to the emergence of experimental clones.

We next investigated whether experimental clones exhibit other indicators of oncogenic transformation. We observed activation of JNK (Figures 2H-2K′) and Src (Figures 2L-2O′) and induction of MMP1 expression (Figures 2P-2S′), as well as activation of the AKT (Figures S2A-S2D′) and MAPK (Figures S2E-S2H′) signaling pathways—all key hallmarks of tumorigenesis—in experimental clones. However, not every cell in each experimental clone showed activation of each marker, and we did observe a degree of variability among clones even in the same intestine. As a result, we were not able to ascertain genotype-dependent differences among experimental genotypes.

We also noted that many of these markers were strongly activated at the clone boundary and, in some cases, in the surrounding wild-type tissue. Non-autonomous pathway activation surrounding experimental clones was most evident with JNK signaling, where all experimental clones resulted in statistically significant non-autonomous activation compared with GFP-only control clones (Figure S2I, also see Figure 2J as an example). We also observed non-autonomous activation of the MAPK pathway in surrounding RPA clones, but the difference was not statistically significant (Figure S2J, also see Figure S2F as an example). Non-autonomous activation of these pathways has been observed during tumorigenesis, cell competition, and compensatory proliferation in multiple experimental contexts, including the *Drosophila* intestine.[34-38] The absence of significant genotype-dependent differences in non-autonomous pathway activation (Figure S2I) indicates a shared niche response to the emergence of transformed clones. Combined, these data demonstrate that transformed clones capture important aspects of tumorigenesis.

Stem cell regulation and cell fate decisions are disrupted within transformed clones

Next, we used well-established markers for different intestinal cell lineages to analyze the cell-type composition of transformed clones to determine whether cancer-driving genetic alterations have an impact on the ability of targeted ISCs to differentiate. Using a custom CellProfiler pipeline, we counted the number of cells carrying each lineage marker in control and experimental clones at two different time points and normalized the numbers to clone volume to account for differences in clone size. Due to antibody compatibility issues, this analysis was conducted separately for each cell fate marker.

All normal intestinal cell lineages were present in transformed clones (Figures 3 and S3). The relative abundance of ISCs and enteroblasts (EBs), which are EC progenitors, varied across genotypes, but we did not observe statistically significant differences between controls and transformed clones (Figures 3A, 3B, and S3A-S3H′). Transformed clones did have a higher abundance of differentiated absorptive ECs 1 week after induction, but the difference reached statistical significance only for RPA and RPPA (Figures 3C and S3I-S3L′). Notably, transformed clones are significantly larger than controls (Figure 1H); as a result, even in cases where the relative abundance of a particular lineage is similar across genotypes (e.g., ISCs; Figures 3A and S3A-S3D′), their number is much higher in transformed clones.

Of all the intestinal cell lineages, we observed the most significant differences in the relative abundance of hormone-secreting EEs 2 weeks after induction (Figure 3D). For instance, RPPA clones had a significantly higher abundance of EEs 2 weeks after induction compared with control clones at the same time point (Figure 3D). These clones also had a significant increase in relative EE abundance over time (Figure 3D; 1 week to 2 weeks comparison). Representative images of clones used in the cell-lineage analysis are presented in Figures 3E-3H′ for EEs and in Figure S3 for the other cell types. This analysis demonstrates that transformed clones include all cell types typically found in the wild-type intestine (Figures 3I and 3J). The larger size of transformed clones and the changes we observed in the relative EE and EC abundances suggest a significant disruption of stem cell regulation and cell fate decisions within transformed tissue.

Transformed clones include cells that co-express multiple cell fate markers

In our cell-lineage analysis, we noted the presence of many EE cells in transformed clones that exhibited a low level of Prospero (Pros) staining intensity compared with the surrounding wild-type tissue and in control clones (e.g., Figure 3G′). We hypothesized that some of these cells may be products of abnormal EE differentiation. To explore this further, we performed a series of co-stainings to investigate whether EEs that co-express other cell fate markers are present in experimental clones (Figures 4 and S4). We found that approximately 5% of large RPA clones contained cells positive for both ISC and EE markers, while no such cells were present in control clones (Figures 4A-4F and 4M).

EE differentiation in the normal intestine starts with an asymmetric ISC division, which produces an EE progenitor (EEP) that expresses low levels of *Dl-LacZ* () and Pros, which then undergoes one round of cell division to generate a pair of EEs or, in some cases,

directly differentiates into an EE.[58,59] The absence of *Dl-LacZ*/Pros-positive cells in control clones may reflect their rare nature in the normal intestine. Regardless, an analysis of a comparable number of intestines and clones in all genotypes identified *Dl-LacZ*/Pros-positive cells only within RPA clones. We also confirmed these results with another marker for differentiated EEs, the peptide hormone Tk. RPA clones also had cells that co-expressed Tk and the ISC marker *Dl-LacZ* (Figure S4A).

Cells co-expressing ISC and EE markers were also present in the wild-type tissue near 15% of RPPA clones and 25% of RPMA clones, but not within the clones themselves (Figures 4G-4M), suggesting some genotype-dependent non-autonomous effects on EE differentiation. We also found cells co-expressing EE and EB markers within RPA and RPMA clones and the surrounding wild-type epithelium, while such cells were absent in controls and RPPA clone bearing intestines (Figures 4M and S4B-S4E″). Combined, these findings suggest that cancer-driving genetic alterations induce disruptions in EE differentiation and cell fate.

Transformed cells that co-express multiple cell fate markers may be products of abnormal differentiation. Alternatively, their presence may reflect the more dynamic and fluid nature of cell fates within transformed tissue, where individual cells can dedifferentiate to more stem-like states. Our observation that cells co-expressing ISC and EE markers had relatively low signal intensity for both markers, compared with controls or cells that express a single cell fate marker, is consistent with both possibilities. To further explore these questions, we used our PS platform to target our multigenic combinations directly to differentiated EEs, using *pros-gal4* to determine whether differentiated EEs can give rise to multicellular clones (Figure 5).

Almost all individual EEs targeted using *PS* and *pros-gal4* resulted in small, single-celled clones (Figures 5A and 5B; representative images in Figures 5C-5F). We did observe rare multicellular control clones at later time points (Figure 5B), which may be products of rare EEPs, so we cannot rule out the possibility that some EEPs may express *pros-gal4*. Still, our analysis suggests that the *pros-gal4>PS* system predominantly or exclusively targets differentiated EEs. Consistent with this, all GFP-positive cells in *pros-gal4>PS* intestines showed strong Pros expression (Figures 5G and 5G′), but we did not find any that also expressed Dl (see Figure S5A as an example).

Individual EEs targeted with our multigenic models using *PS* and*pros-gal4*, on the other hand, resulted in a significant number of multicellular clones (Figure 5B). Consistent with their cell of origin, all GFP-positive cells expressed the EE marker Pros (Figures 5D-5J′). We did note a downward trend in the number of multicellular clones induced by our multigenic models over time (Figure 5B), indicating that EE-derived multicellular clones do not survive as long or proliferate as much as those derived from esg^{+} cells. Despite the resulting clones' small size and shorter life span, these results demonstrate that cancer-driving genetic alterations can confer proliferative abilities to EEs.

We next tested whether any of the resulting transformed cells also expressed stem cell markers. None of the GFP-positive cells in GFP-only controls or RPPA or RPMA clones

expressed Dl (Figures S5A-S5C), but rare cells positive for the ISC marker Dl were present in RPA clones (Figure S5D). This is significant, as RPA is the only genotype where we found *Dl-LacZ*$^{+}$/Pros^{+} cells in transformed clones generated by targeting stem/progenitor cells (Figures 4D-4F and 4M). These findings illustrate genotype-dependent differences in EEs' ability to form multicellular clones.

As our analysis relies on immunohistochemical analysis of a small number of cell fate markers, it is difficult to conclusively say that these transformed EEs are products of dedifferentiation that acquired stem cell characteristics. Still, our findings point to significant disruptions in EE cell fate. Notably, EE dedifferentiation has been reported to contribute to mammalian intestinal regeneration in response to injury and inflammation and the development of small intestinal neuroendocrine tumors, but a role in colorectal cancer progression has not been demonstrated.[60] Additional studies will be required to determine whether the cells we observe in these clones reflect actual dedifferentiation events and whether there are additional disruptions in cell fate that could have been missed using available cell fate markers.

Transformed EEs promote clone growth through multiple mechanisms

To investigate whether EEs contribute to the growth of transformed clones, we attempted to deplete EE cells in our clones by knocking down *scute (sc)*, a transcription factor required for EE differentiation in the adult *Drosophila* intestine.[61] *sc* knockdown significantly reduced EE cell number within control, RPPA, and RPMA clones, but surprisingly did not affect EE cells within RPA clones (Figure 6A). Pros^{+} EE cells persisted in RPA clones upon *sc* knockdown (Figure 6B-6C′), indicating that EE cell fate within RPA clones does not require this master regulator of EE cell fate. We confirmed these results using an antibody against the EE peptide hormone Tk[62]; *sc* knockdown did not reduce Tk-expressing EEs in RPA clones (Figures 6D-6F). On the other hand, *sc* knockdown eliminated Dl^{+}/Tk^{+} cells we have previously described in RPA clones (Figures 6G-6H″, also see Figure S4A), indicating that *sc* is required for this mixed cell fate with both EE and ISC characteristics.

We next investigated whether EEs play a role in transformed clone growth. Genetic depletion of EEs resulted in a significant reduction in RPMA clone size (Figure 6I), indicating a tumor-promoting role. Consistent with the continued presence of the EE cells in RPA clones, *sc* knockdown did not affect the size of RPA clones. Surprisingly, we also found no difference in RPPA clone size, despite a significant reduction in EE cell numbers (Figures 6A and 6I). Interestingly, we frequently observed GFP-negative, Pros^{+}, and Tk^{+} wild-type EE cells trapped inside large, EE-depleted RPPA clones (Figures 6J and 6K). We did not observe such cells in the absence of *sc* knockdown in RPPA clones or any other genotype, with or without *sc* knockdown. These findings suggest that, at least in the case of RPPA, transformed clones can adapt to EE loss by appropriating niche signals secreted by wild-type EE cells. It is unclear whether EE-depleted RPPA clones actively recruit and trap wild-type EE cells or only those that emerge close to wild-type EE cells can give rise to large clones. Either way, these findings emphasize the ability of transformed cells to adapt to changes in their cell-type composition by diverting niche signals from their environment to support their growth.

EEs serve a niche function to regulate intestinal homeostasis by secreting signals directed to other cell types, including ISCs, both directly and indirectly.[24-26] We hypothesize that depleting EE cells from transformed clones compromises clone growth by depriving transformed clones of one or more of these secreted molecules. A well-established mechanism by which EE cells regulate intestinal homeostasis is through the peptide hormone Tk,[25,26] one of the most abundant secreted peptides in the adult midgut.[63] As Tk-expressing EEs are present within our transformed clones (Figure 6F), we reasoned that the Tk-mediated feedback mechanism might be appropriated to promote stem cell proliferation and transformed clone growth. Knocking down Tk within transformed clones resulted in a strong reduction in the size of both RPA and RPPA clones (Figure 6L) and the number of ISCs per clone (Figure 6M), demonstrating a tumor-promoting role for this hormone. RPMA clones, on the other hand, were not sensitive to Tk loss (Figures 6L and 6M), suggesting that other secreted signals mediate the tumor-promoting effects of EEs. Notably, RPMA clones had the lowest number of Tk-positive EEs (Figure 6F), which may explain their insensitivity to Tk loss and their relatively small size compared with RPA and RPPA clones (Figure 1H).

In the wild-type intestine, Tk signals the overlying visceral muscle to express and secrete the *Drosophila* insulin-like peptide 3 (Dilp3), which induces ISC proliferation through the insulin receptor (InR).[25] Knocking down InR, which mediates the ISC response to this feedback mechanism, within transformed clones significantly reduced only RPA clone size and ISC number (Figures 6N and 6O). RPPA appears insensitive to this specific feedback mechanism, likely because both MAPK and PI3K pathways, typically activated by the receptor tyrosine kinase InR, are already strongly activated in this model due to oncogenic RAS and PTEN loss.[43] These findings highlight genotype-dependent nuances in how a transformed clone's specific mutation profile dictates its dependence on homeostatic cell-cell communication mechanisms present in its tissue of origin.

Our observation that RPPA clones are still sensitive to Tk knockdown (Figures 6L and 6M) suggests that Tk must contribute to RPPA clone growth by signaling other cell types in the intestine. To determine whether transformed cells themselves respond to transformed EE-derived Tk, we knocked down the Tk receptor TkR99D (TkR) within transformed clones. We found a significant reduction in clone size and ISC number in both RPA and RPPA clones, demonstrating that Tk directly acts on other transformed cells within clones of both genotypes. Previous studies have shown that Tk can signal ECs to regulate lipid metabolism through its receptor TkR; whether Tk-TkR signaling directly regulates ISC proliferation remains to be determined.[24,26] Additional cell-lineage-specific genetic manipulations within transformed clones will be required to determine which transformed cell types directly respond to Tk. Consistent with our results with Tk knockdown (Figures 6L and 6M), TkR knockdown did not affect RPMA clone size or ISC number (Figures 6P and 6Q), further supporting a Tk-independent tumor-promoting mechanism for EEs in this genotype.

Combined, these studies demonstrate that the specific combination of genetic alterations in a transformed cell has an impact on its lineage identity and determines whether and how it responds to niche signals in its environment (Figures 6R and 6S). In RPA clones, we propose that the Tk hormone secreted from transformed EEs induces ISC proliferation

and clone growth directly within transformed clones through its receptor and indirectly by signaling the overlying visceral muscle to induce the expression of Dilp3. In RPPA clones, Tk/TkR signaling within transformed tissue induces ISC proliferation and clone growth either directly by acting in ISCs or indirectly through other cell lineages within transformed clones; however, feedback through the Tk/Dilp3/InR axis is not required. In RPMA clones, the tumor-promoting role of EEs is not mediated by Tk, suggesting a role for other secreted ligands.

EEs in the intestine secrete a large number of hormones that regulate intestinal homeostasis as well as organismal metabolism.[13,14] Furthermore, intestinal cells use a large repertoire of secreted signaling molecules to communicate with one another and regulate intestinal homeostasis (Figure 6R). We next investigated whether transformed clones drive changes in the expression of EE peptide hormones and signaling molecules used for cell-cell and interorgan communication by analyzing the expression level of 7 EE-derived peptide hormones and 14 signaling molecules by qPCR. Intestines bearing transformed clones of all three genotypes express significantly higher levels of the EE peptide hormones AstA, AstC, and NPF (Figures S5A-S5C); *Drosophila* JAK/STAT ligand *upd3*; and the EGF ligand *spi* (Figures S5D-S5F). We also observed genotype-dependent changes in the expression of several other hormones (Figures S5A-S5C) and signaling molecules relevant to intestinal homeostasis (Figures S5G-S5I).

Previous studies with ISC clones revealed the importance of signals from the microenvironment to support tumor growth.[34,35,64] Specific transformed cell lineages expressing these hormones and signaling molecules, as well as their potential roles in tumorigenesis, intestinal homeostasis, interorgan communication, and whole animal metabolism, need to be functionally interrogated in future studies. We hypothesize that transformed clones that reflect the cell-type heterogeneity of their tissue of origin may produce many of the previously identified niche signals tumor autonomously, reducing their dependence on their microenvironment. Understanding such context-dependent nuances and their impact during intestinal transformation could identify novel vulnerabilities and druggable regulatory nodes to be exploited for targeted therapy in specific genetic contexts.

DISCUSSION

Here, we report a new genetic platform, PS, designed to target transgene expression to a small subset of cells expressing any tissue/cell-type-specific Gal4 of interest. We have used it to study stem cell regulation and cell-cell interactions during intestinal transformation in discrete clones where cell-lineage heterogeneity is preserved. PS is a flexible platform that can be combined with any gal4 of interest to achieve more refined and permanent genetic manipulations. For instance, it could be used to reduce the number of targeted cells in other disease models to better study their interactions with their environment. It also has broad applications beyond disease modeling; it would be particularly effective for stem cell and developmental biology studies in which cells of interest often shut down the expression of cell-type/tissue-specific *gal4* lines as part of their developmental and differentiation program.

Like most epithelial tumors, colorectal cancer is a genetically complex and heterogeneous disease where concurrent deregulation of multiple cancer-relevant pathways is common.[39] Stem cell function and, more broadly, epithelial homeostasis is regulated by complex interactions that integrate short- and longer-range signals with intrinsic, lineage-specific properties of individual cells. These intercellular signaling mechanisms are then disrupted by cancer-driving genetic alterations in context-dependent and often unpredictable ways and can also be appropriated to support tumor growth. The experimental platform we describe here provides an opportunity to study these complex interactions in a whole-animal setting using a model system with powerful genetic tools available for mechanistic studies. The genotype-dependent nuances in molecular mechanisms underlying the tumor-promoting role we uncovered for the EE lineage in our multigenic models (Figure 6S) illustrate the utility and power of this experimental system.

Multiple lines of evidence from our work point to disruptions in EE differentiation and alterations in EE identity in RPA clones: (1) we find cells co-expressing EE and ISC markers Pros and Dl, respectively, and Dl^+ cells that express the EE hormone Tk; (2) the EE cell fate in RPA clones does not depend on the transcription factor *sc*, which is required for EE differentiation in the wild-type intestine[61]; and (3) direct targeting of EEs with the RPA multigenic combination results in small, multicellular clones, which include cells that express the ISC marker Dl. The absence of such cells in RPMA and RPPA clones suggests that loss of TGF-β signaling and PI3K hyperactivation can independently alter EE cell fate. TGF-β signaling has been shown to drive dedifferentiation and promote ISC properties in human colorectal cancer[65]; so, the alterations we observe in our system may also reflect dedifferentiation events. Subsequent studies using additional cell fate markers will be necessary to explore this possibility further. The role of PI3K signaling in dedifferentiation is more complex and context dependent, where PI3K pathway activation can lead to stem cell exhaustion and terminal differentiation or promote dedifferentiation and stemness in various cancers, including CRC.[66] Overall, these findings demonstrate that the cell-lineage composition of transformed clones and disruptions in EE cell fate are dictated by the specific combination of cancer-driving genetic alterations they carry.

Previous clinical observations point to a tumor-promoting role for EEs in colon cancer[27,29,30]; however, the mechanisms underlying this effect have remained elusive. Significantly, the EE subtype associated with worse prognosis and lower survival rates in colorectal cancer patients expresses Tac1, the human ortholog of Tk[28-30,67]; however, a role for Tac1 in this process has not been demonstrated. Together with our results, these observations suggest that EEs can act as regulators of ISC proliferation, likely through multiple mechanisms, and that the tumor-promoting role we identified for the EE hormone Tk is conserved. Our work highlights the potential of multilineage differentiation as a potential target for cancer drug discovery approaches and pharmacological manipulation of EE fate or abundance as a possible treatment strategy for colorectal cancer. Furthermore, as many of the EE hormones upregulated in transformed clone-bearing intestines (Figure S6) are also known to signal the brain and other organs,[68,69] these changes in EE hormone expression could have a significant impact on other organs and whole-animal metabolism, which will need to be investigated in future studies.

Limitations of the study

The PS platform allowed us to generate and study a relatively small number of transformed clones over time. While the induction frequency was relatively constant and comparable across genotypes (Figure S1D), the location of targeted cells remained random. As a result, we observed significant variability in the size and location of transformed clones. This type of variability is also commonly observed in human colon tumors,[70,71] so while not surprising, it introduces a degree of variability across experiments that can be challenging. We attempted to mitigate this problem by analyzing a large number of clones throughout the intestine; future studies exploring regional differences in the behavior of transformed clones can provide additional insights into intestinal transformation.

Although we were able to generate and study transformed clones that reflect the cell-type heterogeneity of the adult *Drosophila* intestine, our cell fate analysis was limited by the availability of cell fate markers and antibody compatibility. As a result, we could not simultaneously evaluate all cell markers in individual clones. Furthermore, relying on immunohistochemistry data can be limiting for analyses of rare cells with mixed lineages. While we tried to mitigate this problem by analyzing large and comparable numbers of clones in all genotypes, more unbiased and higher resolution approaches like single-cell RNA sequencing will be necessary to fully explore the cell fate disruptions induced in transformed clones. Our findings revealed an important role for transformed EEs in supporting transformed growth, but the molecular mechanisms mediating these effects in RPMA clones remain to be resolved. Our qPCR analyses identified several peptide hormones and other secreted molecules that are upregulated in clone-bearing intestines as candidates to be functionally explored in future studies.

STAR★METHODS

RESOURCE AVAILABILITY

Lead contact—Further information and requests for resources should be directed to and will be fulfilled by the lead contact, Erdem Bangi (ebangi@bio.fsu.edu)

Materials availability—Plasmids and Drosophila strains generated in this study are available upon request. Requests for plasmids and Drosophila strains should be directed to and will be fulfilled by the lead contact.

Data and code availability

- All data reported in this paper will be shared by the lead contact upon request.
- This paper does not report original code.
- Any additional information required to reanalyze the data reported in this paper is available from the lead contact upon request.

EXPERIMENTAL MODEL AND STUDY PARTICIPANT DETAILS

All *Drosophila melanogaster* strains were maintained at room temperature on a standard Drosophila medium. Multigenic cancer combinations used in this study are described

previously[43]. Transgenic Drosophila lines used in multigenic cancer combinations are *UAS-ras^{G12V}* (II, G. Halder), and three RNAi lines, *UAS-p53^{RNAi}* (II), *UAS-pten^{RNAi}* (III) and *UAS-apc^{RNAi}* (II), that were obtained from the Vienna Drosophila Resource Center VDRC[72]. Establishment and validation of the multigenic combinations used in this study are described in Bangi et al.[43,44] and Datta et al[44]. Additional transgenic Drosophila lines used in this study were obtained from the Bloomington Drosophila Stock Center (BDSC): *Dl-LacZ* (BDSC #11651), *Su(H)GBE-LacZ* (BDSC #83352), UAS-*sc^{shRNA}* BDSC #26206), UAS-*Tk^{RNAi}* (BDSC #25800), UAS-TkR99D^{RNAi} (BDSC #27513) and *UAS-InR^{RNAi}* (BDSC # 35251).

A third chromosome insertion of the PS construct (line M2, inserted into the attp2 landing site) was incorporated into the background of each cancer model to generate the following fly lines: **1)** *w^{1118} ; UAS-ras^{G12V} UAS-p53^{RNAi} UAS-apc^{RNAi}/CyO; PS attp2 M2/TM6b, Hu, Tb* **2)** *w^{1118} ; UAS-ras^{G12V} UAS-p53^{RNAi} UAS-pten^{RNAi} UAS-apc^{RNAi}//CyO; PS attp2 M2/TM6b, Hu, Tb* and **3)** *w^{1118} ; UAS-ras^{G12V} UAS-p53^{RNAi} UAS-pten^{RNAi} UAS-Med^{RNAi}/CyO; PS attp2 M2/TM6b, Hu, Tb*.

Experimental animals were generated by crossing virgin females from the *w^{1118} UASdcr-2/Y, hs-hid; esg-gal4 tub-gal80^{ts}* or *w^{1118} UASdcr-2/Y, hs-hid; pros-gal4/TM6b, Hu, Tb* to males carrying multigenic combinations and the PS construct listed above. Males carrying the PS construct only were used as controls. The Y chromosome *hs-hid* transgene, which results in ubiquitous activation of apoptosis when induced[73], was used to kill all male progeny and facilitate mass virgin female collection. Crosses were kept at 18°C to prevent transgene expression. When progeny emerged, adult female progeny with the following genotypes were collected: For *esg-gal4*: **1)** *w^{1118} UASdcr-2/w^{1118} ; UAS-ras^{G12V} UAS-p53^{RNAi} UAS-apc^{RNAi}/esg-gal4 tub-gal80^{ts}; PS attp2 M2/+* **2)** *w^{1118} UASdcr-2/ w^{1118} ; UAS-ras^{G12V} UAS-p53^{RNAi} UAS-pten^{RNAi} UAS-apc^{RNAi}/esg-gal4 tub-gal80^{ts}; PS attp2 M2/+* **3)** *w^{1118} UASdcr-2/w^{1118} ; UAS-ras^{G12V} UAS-p53^{RNAi} UAS-pten^{RNAi} UAS-Med^{RNAi}/esg-gal4 tub-gal80^{ts}; PS attp2 M2/+* and **4)** *w^{1118} UASdcr-2/w^{1118} ; +/esg-gal4 tub-gal80^{ts} ; PS attp2 M2/+* as controls. For *pros-gal4*: **1)** *w^{1118} UASdcr-2/w^{1118} ; UAS-ras^{G12V} UAS-p53^{RNAi} UAS-apc^{RNAi}/+; PS attp2 M2/pros-gal4* **2)** *w^{1118} UASdcr-2/w^{1118} ; UAS-ras^{G12V} UAS-p53^{RNAi} UAS-pten^{RNAi} UAS-apc^{RNAi}/+; PS attp2 M2/pros-gal4* **3)** *w^{1118} UASdcr-2/w^{1118} ; UAS-ras^{G12V} UAS-p53^{RNAi} UAS-Med^{RNAi} UAS-apc^{RNAi}/+; PS attp2 M2/pros-gal4* and **4)** *w^{1118} UASdcr-2/w^{1118} ; +/+; PS attp2 M2/pros-gal4* as controls. Clones were induced by placing collected flies at 29°C to inactivate Gal80^{ts}. Experimental animals were transferred onto fresh food three times a week until dissection.

To introduce the Lac-Z and RNAi transgenes into experimental animals, the following fly lines were generated and crossed to males with genotypes listed above: **1)** *w^{1118} UASdcr-2/Y, hs-hid; esg-gal4 tub-gal80^{ts}; Dl-LacZ /TM6b, Hu, Tb* **2)** *w^{1118} UASdcr-2/Y, hs-hid; esg-gal4 tub-gal80^{ts}/CyO; Su(H)-GBE-LacZ /TM6b, Hu, Tb* **3)** *w^{1118} UASdcr-2/Y, hs-hid; esg-gal4 tub-gal80^{ts} ; UAS-sc^{shRNA}/S-T, tub-gal80, Cy, Tb, Hu* **4)** *w^{1118} UASdcr-2/Y, hs-hid; esg-gal4 tub-gal80^{ts} ; UAS-Tk^{RNAi}/S-T, tub-gal80, Cy, Tb, Hu*, **5)** *w^{1118} UASdcr-2/Y, hs-hid; esg-gal4 tub-gal80^{ts} ; UAS-InR^{RNAi}/S-T, tub-gal80, Cy, Tb, Hu*, and **6)** *w^{1118} UASdcr-2/Y, hs-hid; esg-gal4 tub-gal80^{ts} ; UAS-TkR^{RNAi}/S-T, tub-gal80, Cy, Tb, Hu*

METHOD DETAILS

Plasmid construction and transgenesis—PromotorSwitch transgene was first digitally assembled using publicly available sequences. Two pieces, [FRT-FRT3-Gal80^{ts}-FRT] and [Gal80-FRT3], were generated by gene synthesis (Genewiz/Azenta). act5C promoter and Gal4 coding sequences were amplified from the CoinFLP plasmid (Addgene 52890)[52] as two separate fragments. All four fragments were sequentially cloned into pUC57-Kan by standard restriction cloning methods to generate the final [Act5C-FRT-FRT3-Gal80^{ts}-FRT-Gal80-FRT3] transgene.

To generate the multigenic PS construct that included the [UAS-GFP], [UAS-FLP], and the [Act5C-FRT-FRT3-Gal80^{ts}-FRT-Gal80-FRT3] transgenes, we modified our multigenic vector[56] by removing one of the three UAS cassettes to generate 2xUAS-attB (Figure S1A, and Data S1). We then PCR-amplified FLP and GFP coding sequences from genomic DNA of transgenic flies carrying these transgenes using primers designed to append restriction sites of enzymes NotI and XbaI to the 5’ and 3’ end of the FLP recombinase coding sequence, and BsiWI and AsiSI to the 5’ and 3’ end of the GFP coding sequence, respectively. We cloned the PCR products sequentially into the multiple cloning sites of the two UAS-cassettes of 2xUAS-attB (Figure S1B). Lastly, the [Act5C-FRT-FRT3-Gal80^{ts}-FRT-Gal80-FRT3] fragment was cloned into the multigenic vector from pUC57-Kan using PmeI and AgeI to generate the final multigenic PromoterSwitch plasmid, 2xUAS-attB_PS_UAS-FLP_UAS-GFP (Figure S1B, and Data S2). All inserts in the final plasmid were sequence-confirmed again, and transgenic flies were generated by PhiC31-mediated targeted integration into the *attp40* and *attp2* landing sites on the second and third Drosophila chromosomes, respectively. Both second and third chromosome insertions were functionally validated; we used one of the third chromosome insertions for this work (attp2, line M2).

Immunohistochemistry, imaging, and scoring—Adult female *Drosophila* intestines were dissected in Phosphate Buffered Saline (PBS) and fixed for 15 minutes at room temperature (30 minutes for Dl staining) in ice-cold 4% paraformaldehyde in PBS. Intestines were washed in PBS and blocked in PBGT (PBS containing 0.1% Triton X and 1% normal goat serum) for 1 hour at room temperature, incubated overnight with primary antibodies at 4°C, rinsed in PBS three times, followed by a 1-hour block at room temperature and incubated with secondary antibody for 2 hours at room temperature. Intestines were mounted in VectaShield mounting medium containing DAPI.

Primary antibodies used were; mouse anti-phospho-SAPK/JNK-pThr183/pTyr185 G9 (Cell Signaling Technology, #9255, 1:100), Rabbit anti-phospho-SRC-pTyr419 (Thermo Fisher Scientific, 44-660-G, 1:100), rabbit anti-phospho-Histone-H3-pSer10 (Sigma Aldrich, H0412, 1:1000), rabbit anti-phospho-AKT-pSer505 (Cell Signaling Technology, #4054, 1:1000), mouse anti-MMP1 (DSHB, 3B8D12 1:200), mouse anti-diphospho-ERK1/2 (Sigma Aldrich, M8159, 1:1000), rabbit anti-beta galactosidase (Thermo Fisher Scientific, # A-11132, 1:200), mouse anti-Prospero (DSHB, MR1A, 1:50), mouse anti-Nubbin (DSHB, 2D4, 1:50) and rabbit anti-Tachykinin (a generous gift from Dr. Jan A. Veenstra The

University of Bordeaux, 1:1000). Alexa 568- or 633-conjugated goat-anti-mouse and goat-anti-rabbit antibodies were used as secondary antibodies at 1:1000.

Fluorescence images were captured using Leica TCS SPE-II DM6 confocal microscope under a 40X objective and processed using Leica LAS-AF software. Additional processing required for quantification was performed using Fiji Image J Software[74]. Approximately 20 flies were dissected for each genotype, and over 100 clones were analyzed for each experiment. Results were confirmed using an independent set of experiments.

Quantification of clone size and cell lineage composition using CellProfiler —Quantifications were performed using CellProfiler, an open-source cell image analysis software developed at the Broad Institute of MIT and Harvard for automated quantitative analyses of phenotypes from image data[75,76]. CellProfiler provides a series of image-processing modules that can be combined and adjusted to generate custom-designed pipelines for different image-based analyses. We generated customized pipelines to quantify the overall clone volume (GFP), the total number of cells in each clone (DAPI), the number of ISCs, EBs, EEs and EEs per clone (sepa-rately) and non-autonomous pathway activity surrounding clones, all of which are available upon request. Briefly, GFP+ clones and DAPI+ cells were identified using the MedianFilter algorithm. DAPI and GFP segmentations were overlaid using the OverlayObjects module, and clone sizes were quantified in voxels from confocal Z-stacks using the MeasureObjectSizeShape module. The number of nuclei per clone was quantified using the RelateObjects algorithm and the output from the overlayobjects module. For analyses including staining for cell lineage markers, the GFP channel, the channel containing the cell lineage markers, and the DAPI channel were segmented using the Watershed algorithm and processed using the OverlayObjects module. Then the RelateObjects algorithm was also used to quantify the number of each cell type per clone. To quantify the non-autonomous pJNK activity, the MedianFilter module was used to identify GFP+ clones and the pJNK signal. The watershed median was used to segment clones and the pJNK signal individually. Next, the MaskImage module was used to mask the GFP channel containing the clones. The OverlayObjects module was then used on the mask and pJNK images, and the MeasureObjectSizeShape module was used to quantify in voxels the volume of the pJNK channel in GFP− cells surrounding the clones.

qPCR analysis—RNA extractions from dissected adult intestines (15 intestines/biological replicate; 3 biological replicates/genotype) or whole larvae (6 larvae/biological replicate; 3 biological replicates/genotype) were performed using the E.Z.N.A. Total RNA Kit I with the RNase-free DNase Set for on-column DNA digestion from the RNA Clean and Concentrator kit following the manufacturer's instructions. For qPCR analysis, 1 μg of RNA from each sample was converted to complementary DNA (cDNA) using the SuperScript III first-strand synthesis kit, and qPCR was performed using the PerfeCTa SYBR Green FastMix for IQ (VWR Scientific). Housekeeping gene *rpl32* was utilized. qPCR data were analyzed using the ΔΔC(t) method[44,77]. Primers used for the qPCR analysis are provided in Table S1.

QUANTIFICATION AND STATISTICAL ANALYSIS

Details of the statistical analyses and quantification can be found in the relevant sections of the methods and Figure legends.

Supplementary Material

Refer to Web version on PubMed Central for supplementary material.

ACKNOWLEDGMENTS

This study used transgenic RNAi lines (Office of the Director R24 OD030002: “TRiP resources for modeling human disease”) obtained from the Bloomington Drosophila Stock Center (NIH P40OD018537) and the Vienna Drosophila Resource Center (VDRC; www.vdrc.at) and monoclonal antibodies obtained from the Developmental Studies Hybridoma Bank, created by the NICHD of the NIH and maintained at The University of Iowa, Department of Biology, Iowa City, Iowa 52242. We thank Alexander Teague for essential discussions and technical assistance during the early stages of this work. We thank Jason Cassara, Justin Brown, Eric Cruz, Sneha Kapil, Autumn Hawkins, Carson Caddy, Dr. Brian Washburn, Dr. Diego Zorio, and Cheryl Pye at the Florida State University Department of Biological Science Molecular Cloning Core Facility for technical support. This work was supported by startup funds from Florida State University and by National Institutes of Health grants R03 CA219321 (E.B.) and R21 GM141734 (E.B.).

REFERENCES

1. Das D, Fletcher RB, and Ngai J (2020). Cellular mechanisms of epithelial stem cell self-renewal and differentiation during homeostasis and repair. Wiley Interdiscip. Rev. Dev. Biol 9, e361. 10.1002/wdev.361. [PubMed: 31468728]
2. Prasetyanti PR, and Medema JP (2017). Intra-tumor heterogeneity from a cancer stem cell perspective. Mol. Cancer 16, 41. 10.1186/s12943-017-0600-4. [PubMed: 28209166]
3. Dalerba P, Kalisky T, Sahoo D, Rajendran PS, Rothenberg ME, Leyrat AA, Sim S, Okamoto J, Johnston DM, Qian D, et al. (2011). Single-cell dissection of transcriptional heterogeneity in human colon tumors. Nat. Biotechnol 29, 1120–1127. 10.1038/nbt.2038. [PubMed: 22081019]
4. Kamińska K, Szczylik C, Bielecka ZF, Bartnik E, Porta C, Lian F, and Czarnecka AM (2015). The role of the cell-cell interactions in cancer progression. J. Cell Mol. Med 19, 283–296. 10.1111/jcmm.12408. [PubMed: 25598217]
5. Das PK, Islam F, and Lam AK (2020). The Roles of Cancer Stem Cells and Therapy Resistance in Colorectal Carcinoma. Cells 9. 10.3390/cells9061392.
6. Nguyen HT, and Duong HQ (2018). The molecular characteristics of colorectal cancer: Implications for diagnosis and therapy (Review). Oncol. Lett 16, 9–18. 10.3892/ol.2018.8679. [PubMed: 29928381]
7. Zheng Z,Yu T, Zhao X, Gao X, Zhao Y, and Liu G (2020). Intratumor heterogeneity: A new perspective on colorectal cancer research. Cancer Med. 9, 7637–7645. 10.1002/cam4.3323. [PubMed: 32853464]
8. Kikutake C, Yoshihara M, Sato T, Saito D, and Suyama M (2018). Pan-cancer analysis of intratumor heterogeneity associated with patient prognosis using multidimensional measures. Oncotarget 9, 37689–37699. 10.18632/oncotarget.26485. [PubMed: 30701024]
9. Boumard B, and Bardin AJ (2021). An amuse-bouche of stem cell regulation: Underlying principles and mechanisms from adult Drosophila intestinal stem cells. Curr. Opin. Cell Biol 73, 58–68. 10.1016/j.ceb.2021.05.007. [PubMed: 34217969]
10. Palikuqi B, Rispal J, and Klein O (2022). Good Neighbors: The Niche that Fine Tunes Mammalian Intestinal Regeneration. Cold Spring Harb. Perspect. Biol 14, a040865. 10.1101/cshperspect.a040865. [PubMed: 34580119]
11. Joly A, and Rousset R (2020). Tissue Adaptation to Environmental Cues by Symmetric and Asymmetric Division Modes of Intestinal Stem Cells. Int. J. Mol. Sci 21, 6362. 10.3390/ijms21176362. [PubMed: 32887329]

12. Haber AL, Biton M, Rogel N, Herbst RH, Shekhar K, Smillie C, Burgin G, Delorey TM, Howitt MR, Katz Y, et al. (2017). A single-cell survey of the small intestinal epithelium. Nature 551, 333–339. 10.1038/nature24489. [PubMed: 29144463]
13. Hung R-J, Hu Y, Kirchner R, Liu Y, Xu C, Comjean A, Tattikota SG, Li F, Song W, Ho Sui S, and Perrimon N (2020). A cell atlas of the adult midgut. Proc. Natl. Acad. Sci. USA 117, 1514–1523. 10.1073/pnas.1916820117. [PubMed: 31915294]
14. Guo X, Yin C, Yang F, Zhang Y, Huang H, Wang J, Deng B, Cai T, Rao Y, and Xi R (2019). The Cellular Diversity and Transcription Factor Code of Drosophila Enteroendocrine Cells. Cell Rep. 29, 4172–4185.e5. 10.1016/j.celrep.2019.11.048. [PubMed: 31851941]
15. Cheng L, Baonza A, and Grifoni D (2018). Models of Human Disease. BioMed Res. Int 2018, 7214974. 10.1155/2018/7214974. [PubMed: 30228988]
16. Mohr SE, and Perrimon N (2019). Drosophila melanogaster: a simple system for understanding complexity. Dis. Model. Mech 12, dmm041871. 10.1242/dmm.041871. [PubMed: 31562251]
17. Miguel-Aliaga I, Jasper H, and Lemaitre B (2018). Anatomy and Physiology of the Digestive Tract ofDrosophila melanogaster. Genetics 210, 357–396. 10.1534/genetics.118.300224. [PubMed: 30287514]
18. Perochon J, Yu Y, Aughey GN, Medina AB, Southall TD, and Cordero JB (2021). Dynamic adult tracheal plasticity drives stem cell adaptation to changes in intestinal homeostasis in Drosophila. Nat. Cell Biol 23, 485–496. 10.1038/s41556-021-00676-z. [PubMed: 33972729]
19. Gervais L, and Bardin AJ (2021). Tracheal remodelling supports stem cells. Nat. Cell Biol 23, 580–582. 10.1038/s41556-021-00695-w. [PubMed: 34040165]
20. Capdevila C, Trifas M, Miller J, Anderson T, Sims PA, and Yan KS (2021). Cellular origins and lineage relationships of the intestinal epithelium. Am. J. Physiol. Gastrointest. Liver Physiol 321, G413–G425. 10.1152/ajpgi.00188.2021. [PubMed: 34431400]
21. Osman D, Buchon N, Chakrabarti S, Huang Y-T, Su W-C, Poidevin M, Tsai Y-C, and Lemaitre B (2012). Autocrine and paracrine unpaired signaling regulate intestinal stem cell maintenance and division. J. Cell Sci 125, 5944–5949. 10.1242/jcs.113100. [PubMed: 23038775]
22. Jiang H, Grenley MO, Bravo M-J, Blumhagen RZ, and Edgar BA (2011). EGFR/Ras/MAPK signaling mediates adult midgut epithelial homeostasis and regeneration in Drosophila. Cell Stem Cell 8, 84–95. 10.1016/j.stem.2010.11.026. [PubMed: 21167805]
23. Jiang H, Patel PH, Kohlmaier A, Grenley MO, McEwen DG, and Edgar BA (2009). Cytokine/Jak/Stat signaling mediates regeneration and homeostasis in the Drosophila midgut. Cell 137, 1343–1355. 10.1016/j.cell.2009.05.014. [PubMed: 19563763]
24. Liu Y, Li JSS, Rodiger J, Comjean A, Attrill H, Antonazzo G, Brown NH, Hu Y, and Perrimon N (2022). FlyPhoneDB: an integrated web-based resource for cell-cell communication prediction in Drosophila. Genetics 220, iyab235. 10.1093/genetics/iyab235. [PubMed: 35100387]
25. Amcheslavsky A, Song W, Li Q, Nie Y, Bragatto I, Ferrandon D, Perrimon N, and Ip YT (2014). Enteroendocrine cells support intestinal stem-cell-mediated homeostasis in Drosophila. Cell Rep. 9, 32–39. 10.1016/j.celrep.2014.08.052. [PubMed: 25263551]
26. Song W, Veenstra JA, and Perrimon N (2014). Control of lipid metabolism by tachykinin in Drosophila. Cell Rep. 9, 40–47. 10.1016/j.celrep.2014.08.060. [PubMed: 25263556]
27. Swatek J, and Chibowski D (2000). Endocrine cells in colorectal carcinomas. Immunohistochemical study. Pol. J. Pathol 51, 127–136. [PubMed: 11247395]
28. Beumer J, Artegiani B, Post Y, Reimann F, Gribble F, Nguyen TN, Zeng H,Van den Born M,Van Es JH, and Clevers H (2018). Enteroendocrine cells switch hormone expression along the crypt-to-villus BMP signalling gradient. Nat. Cell Biol 20, 909–916. 10.1038/s41556-018-0143-y. [PubMed: 30038251]
29. Jezkova J, Williams JS, Pinto F, Sammut SJ, Williams GT, Gollins S, McFarlane RJ, Reis RM, and Wakeman JA (2016). Brachyury identifies a class of enteroendocrine cells in normal human intestinal crypts and colorectal cancer. Oncotarget 7, 11478–11486. 10.18632/oncotarget.7202. [PubMed: 26862851]
30. Gulubova M, and Vlaykova T (2008). Chromogranin A-serotonin-synaptophysin- and vascular endothelial growth factor-positive endocrine cells and the prognosis of colorectal cancer: an

immunohistochemical and ultrastructural study. J. Gastroenterol. Hepatol 23, 1574–1585. 10.1111/j.1440-1746.2008.05560.x. [PubMed: 18771509]

31. Gunawardene AR, Corfe BM, and Staton CA (2011). Classification and functions of enteroendocrine cells of the lower gastrointestinal tract. Int. J. Exp. Pathol 92, 219–231. 10.1111/j.1365-2613.2011.00767.x. [PubMed: 21518048]
32. Loudhaief R. (2016). Enteroendocrine cells, A potential way to control intestinal stem cell proliferation. Int. J. Stem Cell Res. Ther 3. 10.23937/2469-570x/1410037.
33. Guo X, Lv J, and Xi R (2022). The specification and function of enteroendocrine cells in Drosophila and mammals: a comparative review. FEBS J. 289, 4773–4796. 10.1111/febs.16067. [PubMed: 34115929]
34. Patel PH, Dutta D, and Edgar BA (2015). Niche appropriation by Drosophila intestinal stem cell tumours. Nat. Cell Biol 17, 1182–1192. 10.1038/ncb3214. [PubMed: 26237646]
35. Cordero JB, Stefanatos RK, Myant K, Vidal M, and Sansom OJ (2012). Non-autonomous crosstalk between the Jak/Stat and Egfr pathways mediates Apc1-driven intestinal stem cell hyperplasia in the Drosophila adult midgut. Development 139, 4524–4535. 10.1242/dev.078261. [PubMed: 23172913]
36. Patel PH, and Edgar BA (2014). Tissue design: how Drosophila tumors remodel their neighborhood. Semin. Cell Dev. Biol 28, 86–95. 10.1016/j.semcdb.2014.03.012. [PubMed: 24685612]
37. Suijkerbuijk SJE, Kolahgar G, Kucinski I, and Piddini E (2016). Cell Competition Drives the Growth of Intestinal Adenomas in Drosophila. Curr. Biol 26, 428–438. 10.1016/j.cub.2015.12.043. [PubMed: 26853366]
38. Parvy J-P, Hodgson JA, and Cordero JB (2018). as a Model System to Study Nonautonomous Mechanisms Affecting Tumour Growth and Cell Death. BioMed Res. Int 2018, 7152962. 10.1155/2018/7152962. [PubMed: 29725601]
39. Cancer Genome Atlas Network (2012). Comprehensive molecular characterization of human colon and rectal cancer. Nature 487, 330–337. 10.1038/nature11252. [PubMed: 22810696]
40. Gao J, Aksoy BA, Dogrusoz U, Dresdner G, Gross B, Sumer SO, Sun Y, Jacobsen A, Sinha R, Larsson E, et al. (2013). Integrative analysis of complex cancer genomics and clinical profiles using the cBioPortal. Sci. Signal 6, 11. 10.1126/scisignal.2004088.
41. Capo F, Wilson A, and Di Cara F (2019). The Intestine of Drosophila melanogaster: An Emerging Versatile Model System to Study Intestinal Epithelial Homeostasis and Host-Microbial Interactions in Humans. Microorganisms 7, 336. 10.3390/microorganisms7090336. [PubMed: 31505811]
42. Zwick RK, Ohlstein B, and Klein OD (2019). Intestinal renewal across the animal kingdom: comparing stem cell activity in mouse and Drosophila. Am. J. Physiol. Gastrointest. Liver Physiol 316, G313–G322. 10.1152/ajpgi.00353.2018. [PubMed: 30543448]
43. Bangi E, Murgia C, Teague AGS, Sansom OJ, and Cagan RL (2016). Functional exploration of colorectal cancer genomes using Drosophila. Nat. Commun 7, 13615. 10.1038/ncomms13615. [PubMed: 27897178]
44. Datta I, Vassel T, Linkous B, Odum T, Drew C, Taylor A, and Bangi E (2023). A targeted genetic modifier screen in Drosophila uncovers vulnerabilities in a genetically complex model of colon cancer. G3 13, jkad053. 10.1093/g3journal/jkad053. [PubMed: 36880303]
45. Koveitypour Z, Panahi F, Vakilian M, Peymani M, Seyed Forootan F, Nasr Esfahani MH, and Ghaedi K (2019). Signaling pathways involved in colorectal cancer progression. Cell Biosci. 9, 97. 10.1186/s13578-019-0361-4. [PubMed: 31827763]
46. Bertrand FE, Angus CW, Partis WJ, and Sigounas G (2012). Developmental pathways in colon cancer: crosstalk between WNT, BMP, Hedgehog and Notch. Cell Cycle 11, 4344–4351. 10.4161/cc.22134. [PubMed: 23032367]
47. Micchelli CA, and Perrimon N (2006). Evidence that stem cells reside in the adult Drosophila midgut epithelium. Nature 439, 475–479. 10.1038/nature04371. [PubMed: 16340959]
48. Ohlstein B, and Spradling A (2006). The adult Drosophila posterior midgut is maintained by pluripotent stem cells. Nature 439, 470–474. 10.1038/nature04333. [PubMed: 16340960]

49. Medina A, Bellec K, Polcowñuk S, and Cordero JB (2022). Investigating local and systemic intestinal signalling in health and disease with Drosophila. Dis. Model. Mech 15, dmm049332. 10.1242/dmm.049332. [PubMed: 35344037]
50. Liang J, Balachandra S, Ngo S, and O'Brien LE (2017). Feedback regulation of steady-state epithelial turnover and organ size. Nature 548, 588–591. 10.1038/nature23678. [PubMed: 28847000]
51. Wu JS, and Luo L (2006). A protocol for mosaic analysis with a repressive cell marker (MARCM) in Drosophila. Nat. Protoc 1, 2583–2589. 10.1038/nprot.2006.320. [PubMed: 17406512]
52. Bosch JA, Tran NH, and Hariharan IK (2015). CoinFLP: a system for efficient mosaic screening and for visualizing clonal boundaries in Drosophila. Development 142, 597–606. 10.1242/dev.114603. [PubMed: 25605786]
53. Brand AH, and Perrimon N (1993). Targeted gene expression as a means of altering cell fates and generating dominant phenotypes. Development 118, 401–4415. [PubMed: 8223268]
54. McGuire SE, Mao Z, and Davis RL (2004). Spatiotemporal gene expression targeting with the TARGET and gene-switch systems in Drosophila. Sci. STKE 2004, l6. 10.1126/stke.2202004pl6.
55. Theodosiou NA, and Xu T (1998). Use of FLP/FRT system to study Drosophila development. Methods 14, 355–365. 10.1006/meth.1998.0591. [PubMed: 9608507]
56. Bangi E, Ang C, Smibert P, Uzilov AV, Teague AG, Antipin Y, Chen R, Hecht C, Gruszczynski N, Yon WJ, et al. (2019). A personalized platform identifies trametinib plus zoledronate for a patient with KRAS-mutant metastatic colorectal cancer. Sci. Adv 5, eaav6528. 10.1126/sciadv.aav6528. [PubMed: 31131321]
57. Li X, Wu Y, and Tian T (2022). TGF-β Signaling in Metastatic Colorectal Cancer (mCRC): From Underlying Mechanism to Potential Applications in Clinical Development. Int. J. Mol. Sci 23,14436. 10.3390/ijms232214436. [PubMed: 36430910]
58. Zeng X, and Hou SX (2015). Enteroendocrine cells are generated from stem cells through a distinct progenitor in the adult Drosophila posterior midgut. Development 142, 644–653. 10.1242/dev.113357. [PubMed: 25670791]
59. Chen J, Xu N, Wang C, Huang P, Huang H, Jin Z, Yu Z, Cai T, Jiao R, and Xi R (2018). Transient Scute activation via a self-stimulatory loop directs enteroendocrine cell pair specification from self-renewing intestinal stem cells. Nat. Cell Biol 20, 152–161. 10.1038/s41556-017-0020-0. [PubMed: 29335529]
60. Sei Y, Feng J, Zhao X, and Wank SA (2020). Role of an active reserve stem cell subset of enteroendocrine cells in intestinal stem cell dynamics and the genesis of small intestinal neuroendocrine tumors. Am. J. Physiol. Gastrointest. Liver Physiol 319, G494–G501. 10.1152/ajpgi.00278.2020. [PubMed: 32845170]
61. Bardin AJ, Perdigoto CN, Southall TD, Brand AH, and Schweisguth F (2010). Transcriptional control of stem cell maintenance in the Drosophila intestine. Development 137, 705–714. 10.1242/dev.039404. [PubMed: 20147375]
62. Veenstra JA, Agricola H-J, and Sellami A (2008). Regulatory peptides in fruit fly midgut. Cell Tissue Res. 334, 499–516. 10.1007/s00441-008-0708-3. [PubMed: 18972134]
63. Reiher W, Shirras C, Kahnt J, Baumeister S, Isaac RE, and Wegener C (2011). Peptidomics and peptide hormone processing in the Drosophila midgut. J. Proteome Res 10, 1881–1892. 10.1021/pr101116g. [PubMed: 21214272]
64. Mathur D, Bost A, Driver I, and Ohlstein B (2010). A transient niche regulates the specification of Drosophila intestinal stem cells. Science 327, 210–213. 10.1126/science.1181958. [PubMed: 20056890]
65. Nakano M, Kikushige Y, Miyawaki K, Kunisaki Y, Mizuno S, Takenaka K, Tamura S, Okumura Y, Ito M, Ariyama H, et al. (2019). Dedifferentiation process driven by TGF-beta signaling enhances stem cell properties in human colorectal cancer. Oncogene 38, 780–793. 10.1038/s41388-018-0480-0. [PubMed: 30181548]
66. Madsen RR (2020). PI3K in stemness regulation: from development to cancer. Biochem. Soc. Trans 48, 301–315. 10.1042/BST20190778. [PubMed: 32010943]

67. O'Connor TM, O'Connell J, O'Brien DI, Goode T, Bredin CP, and Shanahan F (2004). The role of substance P in inflammatory disease. J. Cell. Physiol 201, 167–180. 10.1002/jcp.20061. [PubMed: 15334652]

68. Yoshinari Y, Kosakamoto H, Kamiyama T, Hoshino R, Matsuoka R, Kondo S, Tanimoto H, Nakamura A, Obata F, and Niwa R (2021). The sugar-responsive enteroendocrine neuropeptide F regulates lipid metabolism through glucagon-like and insulin-like hormones in Drosophila melanogaster. Nat. Commun 12, 4818. 10.1038/s41467-021-25146-w. [PubMed: 34376687]

69. Chen J, Kim S-M, and Kwon JY (2016). A Systematic Analysis of Drosophila Regulatory Peptide Expression in Enteroendocrine Cells. Mol. Cell 39, 358–366. 10.14348/molcells.2016.0014.

70. Overbeek JA, Kuiper JG, van der Heijden AAWA, Labots M, Haug U, Herings RMC, and Nijpels G (2019). Sex- and site-specific differences in colorectal cancer risk among people with type 2 diabetes. Int. J. Colorectal Dis 34, 269–276. 10.1007/s00384-018-3191-7. [PubMed: 30421309]

71. Baran B, Mert Ozupek N, Yerli Tetik N, Acar E, Bekcioglu O, and Baskin Y (2018). Difference Between Left-Sided and Right-Sided Colorectal Cancer: A Focused Review of Literature. Gastroenterology Res. 11, 264–273. 10.14740/gr1062w. [PubMed: 30116425]

72. Dietzl G, Chen D, Schnorrer F, Su K-C, Barinova Y, Fellner M, Gasser B, Kinsey K, Oppel S, Scheiblauer S, et al. (2007). A genome-wide transgenic RNAi library for conditional gene inactivation in Drosophila. Nature 448, 151–156. 10.1038/nature05954. [PubMed: 17625558]

73. Starz-Gaiano M, Cho NK, Forbes A, and Lehmann R (2001). Spatially restricted activity of a Drosophila lipid phosphatase guides migrating germ cells. Development 128, 983–991. 10.1242/dev.128.6.983. [PubMed: 11222152]

74. Schindelin J, Arganda-Carreras I, Frise E, Kaynig V, Longair M, Pietzsch T, Preibisch S, Rueden C, Saalfeld S, Schmid B, et al. (2012). Fiji: an open-source platform for biological-image analysis. Nat. Methods 9, 676–682. 10.1038/nmeth.2019. [PubMed: 22743772]

75. Stirling DR, Swain-Bowden MJ, Lucas AM, Carpenter AE, Cimini BA, and Goodman A (2021). CellProfiler 4: improvements in speed, utility and usability. BMC Bioinf. 22, 433. 10.1186/s12859-021-04344-9.

76. McQuin C, Goodman A, Chernyshev V, Kamentsky L, Cimini BA, Karhohs KW, Doan M, Ding L, Rafelski SM, Thirstrup D, et al. (2018). CellProfiler 3.0: Next-generation image processing for biology. PLoS Biol. 16, e2005970. 10.1371/journal.pbio.2005970. [PubMed: 29969450]

77. Sopko R, Foos M, Vinayagam A, Zhai B, Binari R, Hu Y, Randklev S, Perkins LA, Gygi SP, and Perrimon N (2014). Combining genetic perturbations and proteomics to examine kinase-phosphatase networks in Drosophila embryos. Dev. Cell 31, 114–127. 10.1016/j.devcel.2014.07.027. [PubMed: 25284370]

Highlights

- PromoterSwitch (PS) allows more refined genetic manipulations in *Drosophila*
- Cancer-driving genetic alterations disrupt cell fate decisions in the intestine
- Transformed enteroendocrine cells (EEs) promote intestinal transformation
- The EE hormone Tachykinin supports tumorigenesis through genotype-dependent mechanisms

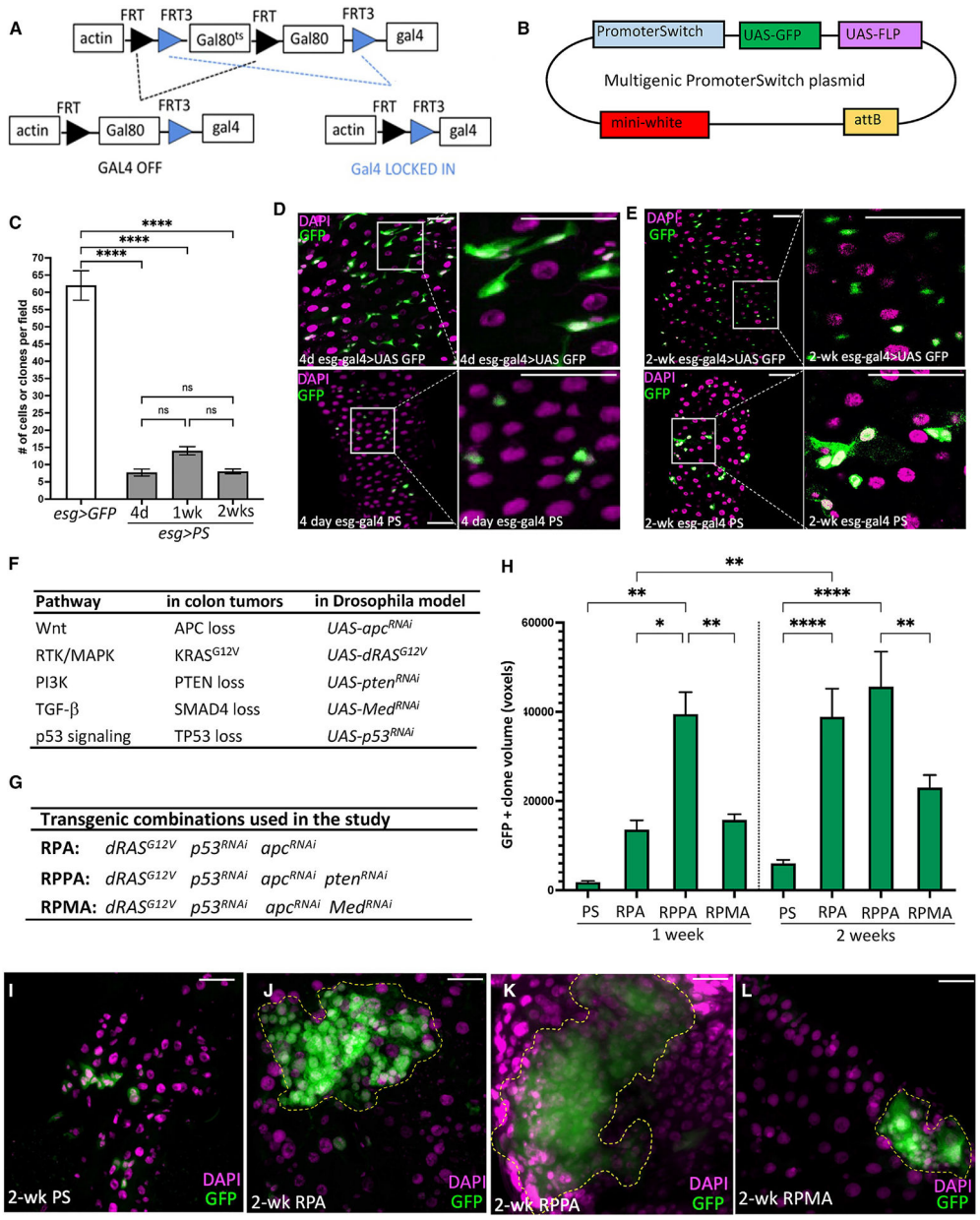

Figure 1. Generating transformed clones in the adult *Drosophila* intestine using PromoterSwitch (PS)

(A) The PS construct is activated by crossing it to a cell-type-specific Gal4 and inactivating Gal80^{ts} with a temperature shift. Once induced from the *UAS-FLP* transgene, FLP recombinase can act on either (1) the FRT pair (black triangles) and excise the Gal80^{ts} coding sequence, bringing the gal80 coding sequence downstream of the actin promoter and irreversibly shutting down the UAS/Gal4 system, or (2) the FRT3 pair (blue triangles) and excise both Gal80^{ts} and Gal80 coding sequences, bringing the gal4 coding sequence downstream of the actin promoter and making UAS-transgene expression independent of the original, cell-type-specific gal4. FRT and FRT3 sequences are incompatible with each other and cannot be paired together in the same excision event.

(B) The PS multigenic plasmid contains the Gal4-inducible *UAS-FLP* and *UAS-GFP* transgenes and the *PS* transgene (A).
(C) Quantification of the number of GFP^+ cells and clones in adult midguts after induction of GFP expression using *esg-gal4* only and with PS at indicated time points.
(D and E) Adult midguts 4 days (D) and 2 weeks (E) after induction of GFP expression using *esg-gal4* only and with PS. Images on the right show magnified regions outlined by the white boxes in the left images. PS allows targeting of a small subset of *esg-gal4*-expressing cells (green, nuclei in magenta) and their subsequent progeny, resulting in small multicellular clones that include large, differentiated cells.
(F) Commonly deregulated pathways in human colon tumors, cancer driver genes selected to represent each pathway, and transgenes used to manipulate their *Drosophila* orthologs.
(G) Transgenic combinations used in this study.
(H–L) Time-course analysis of clone volume (H, n > 100 clones/genotype/time point) and representative images of clones of each genotype used in volume analysis (I–L). Quantifications were performed using a custom-designed pipeline in CellProfiler to determine clone volumes from confocal z stacks (see STAR Methods for details). Clones are in green and nuclei (DAPI) in magenta. Error bars represent the standard error of the mean (SEM); *p ≤ 0.05, **p ≤ 0.01, ****p ≤ 0.0001 (one-way ANOVA with Tukey correction for multiple comparisons, PRISM software). Scale bars: 25 μm. Also see Figure S1 and Data S1 andS2.

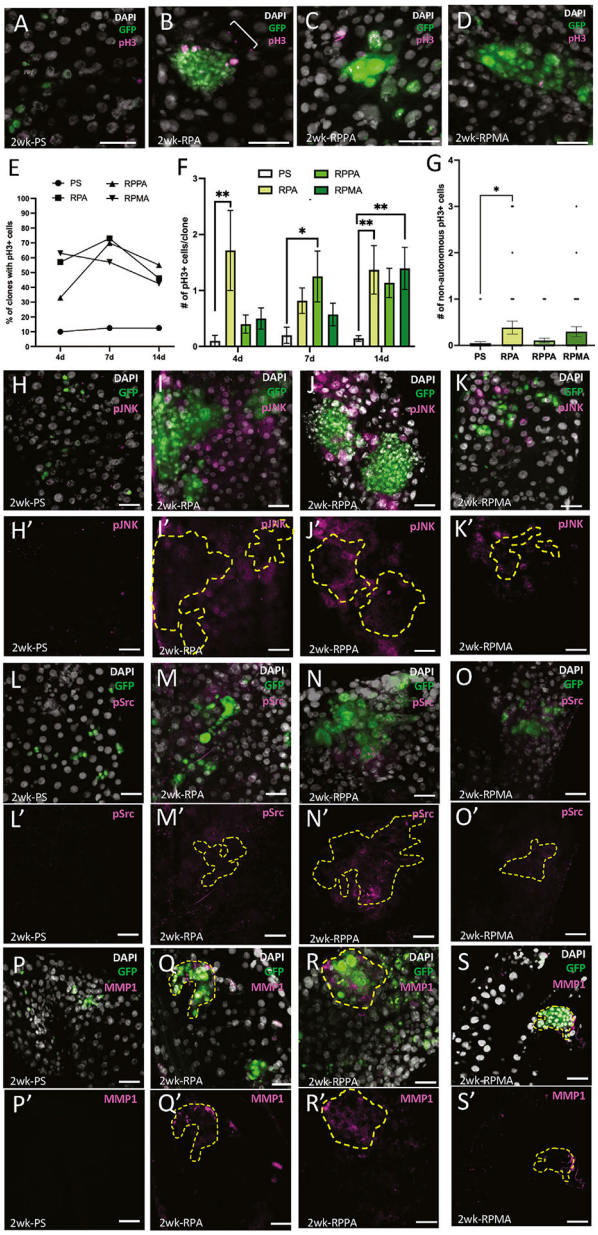

Figure 2. Analysis of tumor hallmarks in experimental clones

(A–D) Representative images of clones for the proliferation analysis using the mitotic marker phospho-Histone 3 (pH3). Clones are in green, nuclei (DAPI) are in gray, and pH3 is in magenta. The bracket in (B) indicates three wild-type pH3+ cells in close proximity to the clone.

(E) Fraction of clones with $pH3^+$ cells.

(F) Number of $pH3^+$ cells/clone.

(G) Number of $pH3^+$ cells in close proximity to the clones (within three nuclei). Error bars represent the standard error of the mean (SEM); *$p \leq 0.05$, **$p \leq 0.01$ (one-way ANOVA with Tukey correction for multiple comparisons, PRISM software).

(H–K′) Phospho-JNK (pJNK) staining in clones (outlined in yellow dashed lines) with indicated genotypes (pJNK in magenta, DAPI in gray, and clones in green).
(L–O′) Phospho-Src (pSrc) staining in clones (outlined in yellow dashed lines) with indicated genotypes (pSrc in magenta, DAPI in gray, and clones in green).
(P–S′) MMP1 staining in clones (outlined in yellow dashed lines) with indicated genotypes (MMP1 in magenta, DAPI in gray, and clones in green).
Scale bars: 25 μm. Also see Figure S2.

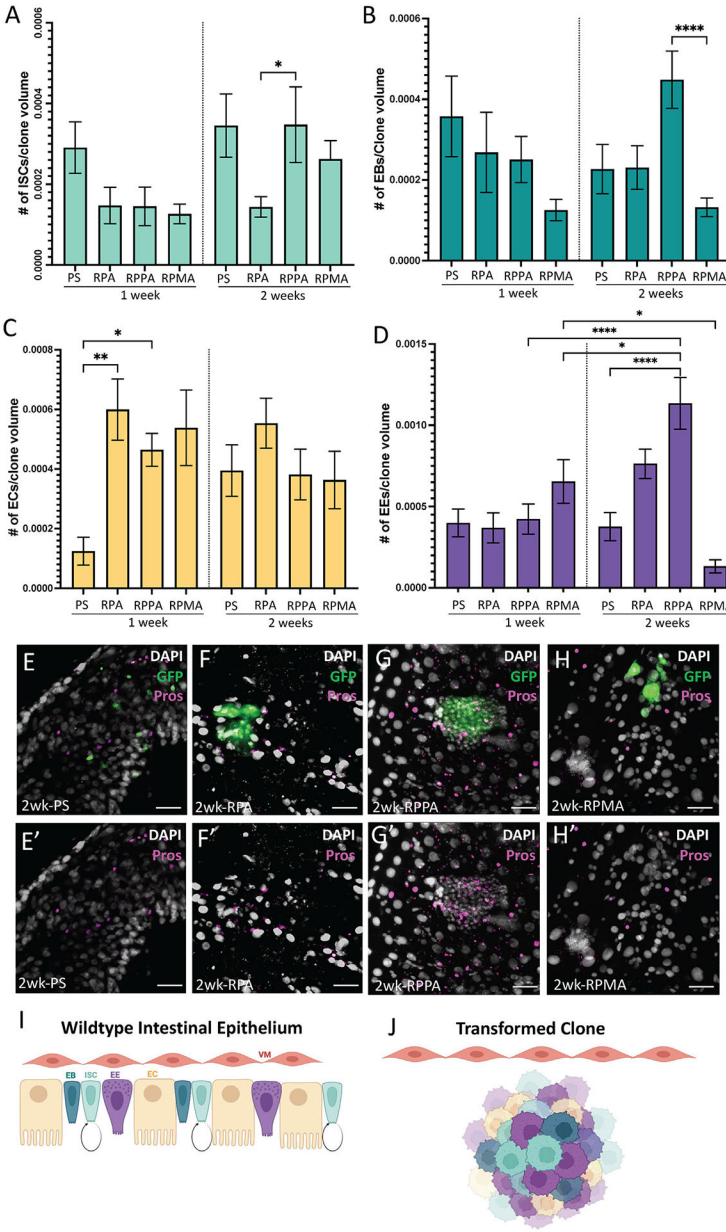

Figure 3. Stem cell regulation and cell fate decisions are disrupted within transformed clones

(A–D) Number of cells positive for the ISC marker *Dl-LacZ* (A), EB marker *Su(H)-GBE-LacZ* (B), EC marker Nubbin (Nub; C), and EE marker Prospero (Pros; D) normalized to the volume of each clone. Error bars represent the standard error of the mean (SEM); *p ≤ 0.05, **p ≤ 0.01, ***p ≤ 0.001, ****p ≤ 0.0001 (one-way ANOVA with Tukey correction for multiple comparisons, PRISM software). Quantifications were performed using a custom-designed pipeline in CellProfiler that counts the number of cells with each lineage marker and the overall 3D volume of each GFP-positive clone from confocal z stacks (see STAR Methods for details).

(E–H′) Representative images of stainings used for the quantification analysis of EE lineage (see Figure S3 for other cell fate markers). Pros is in magenta, clones are in green, and nuclei (DAPI) are in gray. Scale bars: 25 μm.

(I and J) Summary of our findings (made with BioRender). Transformed clones (J) contain all cell lineages found in the normal intestine (I).

Also see Figure S3.

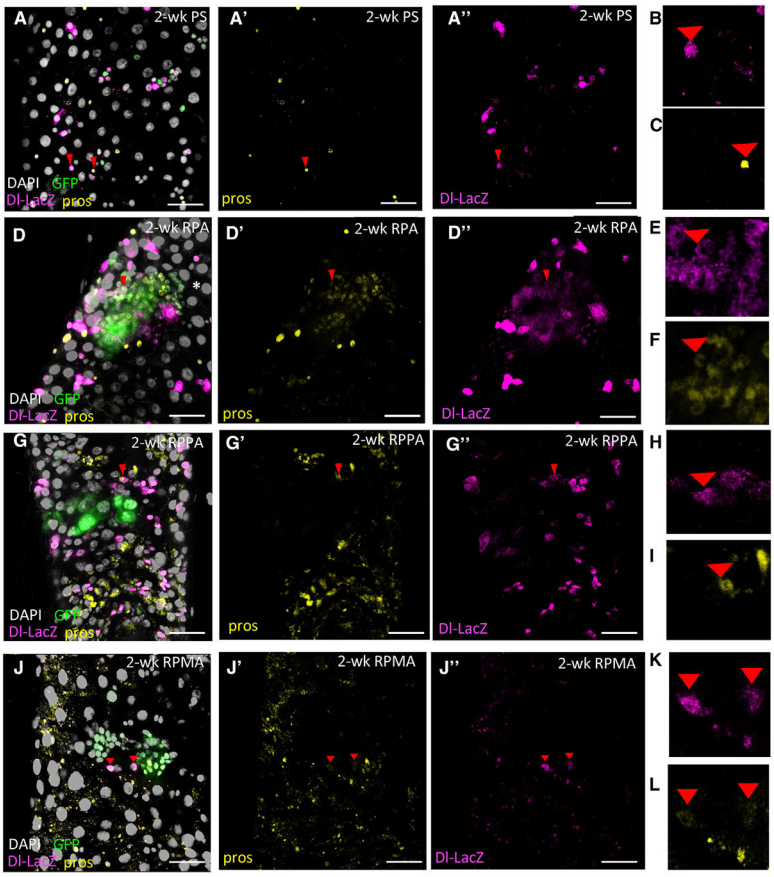

M

Colocalization of EE and ISC/EB cell fate markers			
Markers	**Genotype**	**within clone**	**surrounding clone**
ISC and EE (Dl-LacZ and pros)	**PS**	No	N/A
	RPA	**Yes**	No
	RPPA	No	**Yes**
	RPMA	No	**Yes**
EB and EE (SuH(GBE)-LacZ and pros)	**PS**	No	N/A
	RPA	**Yes**	**Yes**
	RPPA	No	No
	RPMA	**Yes**	**Yes**

Figure 4. Transformed clones include cells that co-express EE and stem/progenitor cell markers

(A–L) Intestines with representative GFP-only control (A–C), RPA (D–F), RPPA (G–I), and RPMA (J–L) clones immunostained for indicated markers. Clones are in green, nuclei (DAPI) are in gray, *Dl-LacZ* is in magenta, Pros is in yellow. Red arrowheads point to cells that co-express *Dl-LacZ* and Pros. Smaller images (B, C, E, F, H, I, K, L) are magnified views of cells highlighted by the arrowheads in (A), (D), (G), and (J). Cells co-expressing *Dl-LacZ* and Pros were observed within but not surrounding RPA clones (D–H) and only surrounding RPPA (G–I) and RPMA (J–L) clones.

(M) Table summarizing cells co-expressing multiple cell fate markers observed within and surrounding clones of each genotype (also see Figure S4).

Scale bars: 25 μm. Also see Figure S4.

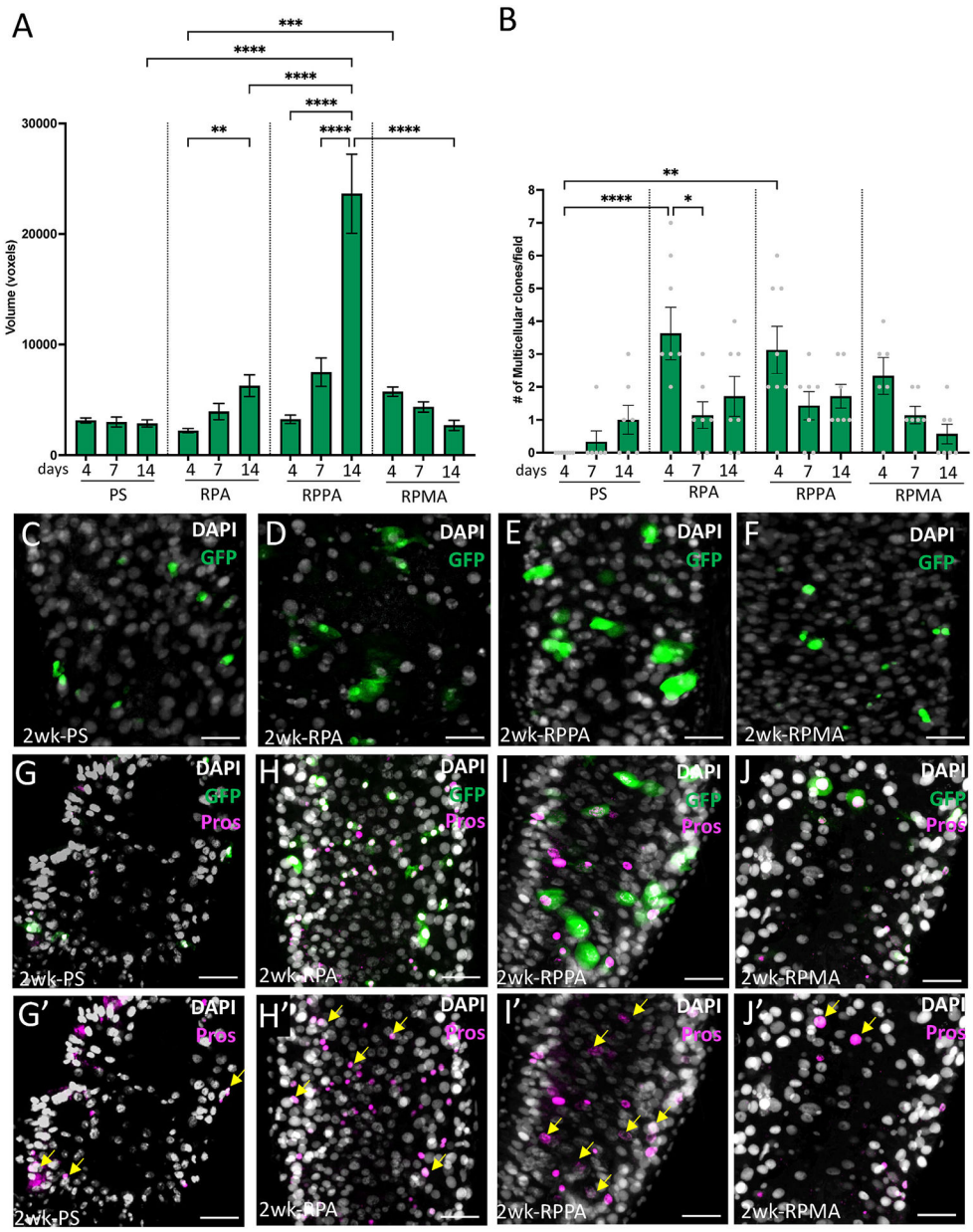

Figure 5. Directly targeting differentiated EEs with multigenic combinations

(A and B) Quantification of clone volume (A) and the number of multicellular clones (B) generated by targeting multigenic combinations to differentiated EEs using *pros-gal4* and PS. Error bars represent the standard error of the mean (SEM); *p ≤ 0.05, **p ≤ 0.01, ***p ≤ 0.001, ****p ≤ 0.0001 (one-way ANOVA with Tukey correction for multiple comparisons, PRISM software).

(C–F) Representative images used in the quantifications presented in (A) and (B).

(G–J·) Targeted EEs and resulting EE-derived clones (green; yellow arrows in G′–J′) express the EE marker Pros (magenta). Nuclei (DAPI) are in gray.

(C–J′) Scale bars: 25 μm.

Also see Figure S5.

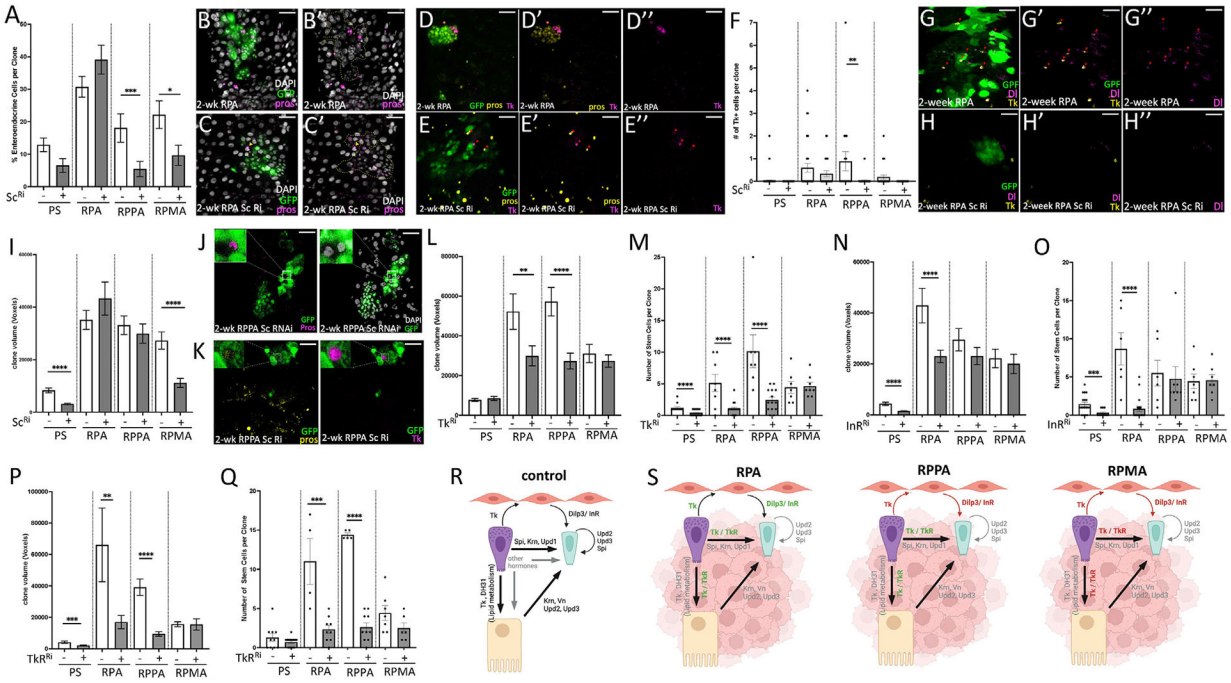

Figure 6. Transformed enteroendocrine cells promote clone growth through multiple mechanisms

(A) Fraction of Pros^{+} EE cells upon *sc* knockdown in control and transformed clones of different genotypes 2 weeks post-induction. Pros^{+} EE cells persist in RPA clones after *sc* knockdown.

(B–C′) An example RPA clone with *sc* knockdown (C, C′) from the dataset used in the quantification presented in (A) with comparable numbers of Pros^{+} EEs to control RPA clones (B, B′). Clones are in green in (B) and (C) and outlined with yellow dashed lines in (B′) and (C′), nuclei (DAPI) are in gray, and Pros is in magenta. Yellow arrowhead: a wild-type EE just outside the clone.

(D–F) Cells expressing the EE peptide hormone Tk are present in RPA clones after *sc* knockdown (red arrows in E–E′) but are significantly reduced upon *sc* knockdown within RPPA clones (F). Clones are in green, Pros is in yellow, and Tk is in magenta. (F) Quantification of the number of Tk-positive cells in control and transformed clones.

(G–H′) Dl and Tk-co-expressing cells observed in RPA clones (G–G′, red arrows, also see Figure S4A) are depleted upon *sc* knockdown. Clones are in green, Tk is in yellow, and Dl is in magenta.

(I) Volume analysis of control and transformed clones of different genotypes with or without *sc* knockdown 2 weeks post-induction (performed using a custom-designed pipeline in CellProfiler to determine clone volumes from confocal z stacks).

(J) An example of a GFP-negative, Pros^{+} (magenta) wild-type EE trapped within an EE-depleted RPPA clone. Nuclei (DAPI) are in gray.

(K) An example of a GFP-negative, Pros^{+} (yellow) wild-type EE expressing Tk (magenta) trapped within an EE-depleted RPPA clone. The top left corner in (J) and (K) shows a magnified view of the GFP-negative cell. Such clones were not observed in control clones, transformed clones of other genotypes, and *sc* wild-type RPPA clones.

(L and M) Volume analysis (L) and the number of stem cells per clone (M) of control and transformed clones with or without *Tk* knockdown 2 weeks post-induction.
(N and O) Volume analysis (N) and the number of stem cells per clone (O) of control and transformed clones with or without *InR* knockdown 2 weeks post-induction.
(P and Q) Volume analysis (P) and the number of stem cells per clone (Q) of control and transformed clones with or without *TkR* knockdown 2 weeks post-induction. (A, H, K–P) Error bars represent the standard error of the mean (SEM); *p ≤ 0.05, **p ≤ 0.01, ***p ≤ 0.001, ****p ≤ 0.0001 (multiple unpaired t tests, PRISM software).
(R and S) Summary of tumor-promoting functions of EEs in different genetic contexts. Mechanisms we found to contribute to transformed clone growth are shown in green, those that are not required in red, and those that have not been explored in this study are in gray. Scale bars: 25 μm.
Also see Figure S6 and Table S1.

KEY RESOURCES TABLE

REAGENT or RESOURCE	SOURCE	IDENTIFIER
Antibodies		
mouse anti-phospho-SAPK/JNK-pThr183/pTyr185 G9	Cell Signaling Technology	Cat #: 9255; RRID:AB_2307321
Rabbit anti-phospho-SRC-pTyr419	ThermoFisher Scientific	Cat #: 44-660-G; RID:AB_2533714
rabbit anti-phospho-Histone-H3-pSer10	Sigma Aldrich	Cat #: H0412; RRID:AB_477043
rabbit anti-phospho-AKT-pSer505	Cell Signaling Technology	Cat #: 4054; RRID:AB_331414
mouse anti-diphospho-ERK1/2	Sigma Aldrich	Cat #: M8159; RRID:AB_477245
mouse anti-MMP1	Developmental Studies Hybridoma Bank	Cat #: 3B8D12; RRID:AB_579781
rabbit anti-beta galactosidase	ThermoFisher Scientific	Cat #: A-11132; RRID:AB_221539
mouse anti-Prospero	Developmental Studies Hybridoma Bank	Cat #: MR1A; RRID:AB_528440
mouse anti-Nubbin	Developmental Studies Hybridoma Bank	Cat #: 2D4; RRID:AB_2722119
rabbit anti- Tachykinin	gift from Dr. Jan A. Veenstra, The University of Bordeaux (Veenstra et al.[62])	N/A
Goat anti-Mouse IgG Secondary Antibody, Alexa Fluor 568	Invitrogen by ThermoFisher Scientific	Cat #: A-11031; RRID:AB_144696
Goat anti-Mouse IgG Secondary Antibody, Alexa Fluor 633	Invitrogen by ThermoFisher Scientific	Cat #: A-21052; RRID:AB_2535719
Goat anti-Rabbit IgG Secondary Antibody, Alexa Fluor 568	Invitrogen by ThermoFisher Scientific	Cat #: A-11036; RRID:AB_10563566
Goat anti-Rabbit IgG Secondary Antibody, Alexa Fluor 633	Invitrogen by ThermoFisher Scientific	Cat #: A-21071; RRID:AB_2535732
Bacterial and virus strains		
Escherichia Coli: Top10	ThermoFisher Scientific	Cat #: C404010
Chemicals, peptides, and recombinant proteins		
Phosphate Buffer Saline 10x	ThermoFisher Scientific	Cat #: J75889-k2
Triton X-100	Acros Organics	Cat #: 32737
Normal Goat Serum	Jackson Immunoresearch	Cat #: 005000121
Vecta Shield	Vector Labs	Cat #: H-1200
paraformaldehyde 16%	ThermoFisher Scientific	Cat #: 28908
Critical commercial assays		
E.Z.N.A Total RNA Kit I	Omega BIO-TEK	Cat #: S1991583
RNA Clean & Concentrator Kit	ZYMO RESEARCH	Cat #: R1013
SuperScript III first-strand synthesis kit	Invitrogen by ThermoFisher Scientific	Cat #: 18080051
Experimental models: Organisms/strains		
D. melanogaster: UAS-ras^{G12V} II	G. Halder	N/A
D. melanogaster: UAS-p53^{RNAi} II	Vienna Drosophila Resource Center	GD-38235
D. melanogaster: UAS-pten^{RNAi} II	Datta et al.[44]	N/A
D. melanogaster: UAS-apc ^{RNAi} II	Vienna Drosophila Resource Center	GD-51468
D. melanogaster: UAS-Med $^{RNAi\ i}$ II	Vienna Drosophila Resource Center	GD-19689
D. melanogaster: UAS-InR ^{RNAi}	Bloomington Drosophila Stock Center	35251
D. melanogaster: Dl-LacZ	Bloomington Drosophila Stock Center	11651
D. melanogaster: Su(H)GBE-LacZ	Bloomington Drosophila Stock Center	83352

REAGENT or RESOURCE	SOURCE	IDENTIFIER
D. melanogaster: UAS-sc^{shRNA}	Bloomington Drosophila Stock Center	26206
D. melanogaster: UAS-Tk ^{RNAi}	Bloomington Drosophila Stock Center	25800
D. melanogaster: UAS-TkR99D ^{RNAi}	Bloomington Drosophila Stock Center	25713
D. melanogaster: w^{1118}; PromoterSwitch (PS) attp2	This study	N/A
D. melanogaster: w^{1118}; UAS-ras^{G12V} UAS-p53^{RNAi} UAS-apc^{RNAi}/CyO; PS attp2/TM6, Hu, Tb	This study	N/A
D. melanogaster: w^{1118}; UAS-ras^{G12V} UAS-p53^{RNAi} UAS-pten^{RNAi} UAS-apc^{RNAi}/CyO; PS attp2/TM6, Hu, Tb	This study	N/A
D. melanogaster: w^{1118}; UAS-ras^{G12V} UAS-p53^{RNAi} UAS-Med^{RNAi} UAS-apc^{RNAi}/CyO; PS attp2/TM6, Hu, Tb	This study	N/A
D. melanogaster: w^{1118} UAS-dcr2/Y[hs-hid]; esg-gal4 tub-gal80^{ts} II	This study	N/A
D. melanogaster: w^{1118} UAS-dcr2/Y[hs-hid]; esg-gal4 tub-gal80^{ts} ; Dl-LacZ/S-T, Cy, Hu, Tb	This study	N/A
D. melanogaster: w^{1118} UAS-dcr2/Y[hs-hid]; esg-gal4 tub-gal80^{ts} ; Su(H)GBE-LacZ/S-T, Cy, Hu, Tb	This study	N/A
D. melanogaster: w^{1118} UAS-dcr2/Y[hs-hid]; pros-gal4 / TM6, Hu, Tb	This study	N/A
Oligonucleotides		
qPCR primers, Table S1	This study	N/A
Recombinant DNA		
pAct-FRT-FRT3-stop-FRT-LexGAD-FRT3-Gal4 attB	Bosch et al.[52]	Addgene, 52890
2xUAS-attB	This study (File S1)	N/A
2xUAS-attB_PS_UAS-FLP_UAS-GFP	This Study (File S2)	N/A
Software and algorithms		
ImageJ	U. S. National Institutes of Health	ImageJ2: 2.3.0/1.53t
CellProfiler	Broad Institute of MIT and Harvard	CellProfiler: 4.2.5
Prism 9.5.0	Graphpad	https://www.graphpad.com/